Title: cAMP-Protein Kinase A and Stress-Activated MAP Kinase signaling mediate transcriptional control of autophagy in fission yeast during glucose limitation or starvation.

Armando Jesús Pérez-Díaz, Beatriz Vázquez-Marín, Jero Vicente-Soler, Francisco Prieto-Ruiz, Teresa Soto, Alejandro Franco, José Cansado* and Marisa Madrid*

Address: Yeast Physiology Group. Department of Genetics and Microbiology. Campus de Excelencia Internacional de Ámbito Regional (CEIR) Campus Mare Nostrum, Universidad de Murcia. 30071 Murcia, Spain.

Corresponding authors: jcansado@um.es; marisa@um.es

Abstract

Macroautophagy/autophagy is an essential adaptive physiological response in eukaryotes induced during nutrient starvation, including glucose, the primary immediate carbon and energy source for most cells. Although the molecular mechanisms that induce autophagy during glucose starvation have been extensively explored in the budding yeast *Saccharomyces cerevisiae*, little is known about how this coping response is regulated in the evolutionary distant fission yeast *Schizosaccharomyces pombe*. Here, we show that *S. pombe* autophagy in response to glucose limitation relies on mitochondrial respiration and the electron transport chain (ETC), but, in contrast to *S. cerevisiae*, the AMP-activated protein kinase (AMPK) and DNA damage response pathway components do not modulate fission yeast autophagic flux under these conditions. In the presence of glucose, the cAMP-protein kinase A (PKA) signaling pathway constitutively represses *S. pombe* autophagy by downregulating the transcription factor Rst2, which promotes the expression of respiratory genes required for autophagy induction under limited glucose availability. Furthermore, the stress-activated protein kinase (SAPK) signaling pathway, and its central mitogen-activated protein kinase (MAPK) Sty1, positively modulate autophagy upon glucose limitation at the transcriptional level through its downstream effector Atf1 and by direct *in vivo* phosphorylation of Rst2 at S292. Thus, our data indicate that the signaling pathways that govern autophagy during glucose shortage or starvation have evolved differently in *S. pombe* and uncover the existence of sophisticated and multifaceted mechanisms that control this self-preservation and survival response.

Keywords

Autophagy; cAMP-protein kinase A; fermentation; glucose; MAP kinase; respiration; *Schizosaccharomyces pombe*; transcription

Abbreviations: AA: Antimycin A; AMPK: adenosine monophosphate-activated protein kinase; ATP: adenosine triphosphate; cAMP-PKA: cyclic adenosine monophosphate-activated protein kinase; cDNA: complementary deoxyribonucleic acid; CESR: core environmental stress response; CFP: cyan fluorescent protein; CFU: colony-forming unit; CR: catabolite repression; DCCD: dicyclohexylcarbodiimide; DHA: dihydroxyacetone; EMM2: Edinburgh minimal medium; ETC: electron transport chain; GFP: green fluorescent protein; Glu: glucose; Gly: glycerol; HA: hemagglutinin; HRP: horseradish peroxidase; MAPK: mitogen-activated protein kinase; mRNA: messenger ribonucleic acid; PAS: phagophore assembly site; RT-qPCR: real-time quantitative polymerase chain reaction; SDS-PAGE: sodium dodecyl sulfate polyacrylamide gel electrophoresis; SAPK: stress-activated protein kinase; TCA: trichloroacetic acid; TOR: target of rapamycin; TORC1: target of rapamycin complex 1; TORC2: target of rapamycin complex 2; TTFA: 2-thenoyltrifluoroacetone; YES: yeast extract supplemented medium.

Introduction

Adaptation to nutrient availability and/or quality changes is crucial for optimal cellular resilience and survival in a changing environment [1]. Glucose, the preferred carbon and energy source, is metabolized by most cells through either fermentation or mitochondrial respiration, which is far more efficient in the energy and biomass generated per glucose molecule. Nevertheless, many organisms, including the budding yeast *Saccharomyces cerevisiae,* use aerobic fermentation instead of respiration for ATP production when glucose is available, a phenomenon known as the "Crabtree effect" [2-5]. The fission yeast *Schizosaccharomyces pombe* is another Crabtree-positive yeast that shows high levels of glycolytic and fermentation enzymes in the presence of a glucose excess, whereas mitochondrial energy metabolism is significantly reduced [6]. Glucose prevents the utilization of alternative carbon sources through a conserved "catabolite repression" (CR) mechanism, which represses transcriptionally the expression of genes involved in the catabolism of less favorable sugars, components of the electron transport chain (ETC), and other mitochondrial proteins [7-10]. Fission yeast CR is mediated by the adenosine monophosphate-activated protein kinase (AMPK) Ssp2 [11-13]. Upon glucose depletion, Ssp2 phosphorylates and triggers the nuclear export of the C_2H_2 zinc finger transcriptional repressor Scr1, which is orthologous to *S. cerevisiae* Mig1 [14,15], to elicit the enhanced expression of catabolite-repressed genes such as *inv1*$^+$ (invertase), *ght5*$^+$ (high-affinity hexose transporter), and *gld1*$^+$ (mitochondrial glycerol dehydrogenase Gld1) [16,17]. Glucose detection by cAMP-PKA signaling also strongly contributes to CR in fission yeast by phosphorylating and negatively regulating the activity of the Zn-finger transcription factor Rst2 [17,18]. Downregulation of cAMP-PKA signaling in glucose-starved cells elicits Rst2 translocation to the nucleus to specifically activate the expression, among others, of genes involved in sexual differentiation and the adaptive growth to non-fermentable carbon sources [19-23]. Moreover, the transcriptional landscape during glucose scarcity is coordinately

regulated by cAMP-PKA signaling and the SAPK pathway [19-23]. Activation of the SAPK effector MAPK Sty1 during glucose limitation or starvation results in the phosphorylation of the bZIP domain transcription factor Atf1 and the induced expression of the Core Environmental Stress Response (CESR) genes, which participate in the adaptive cellular responses to stress [24,25].

Upon glucose exhaustion, yeasts cells undergo a metabolic change from aerobic fermentation to respiratory growth termed the "diauxic shift" [26]. Still, the metabolism of non-glucose carbon sources such as ethanol or glycerol differs considerably in *S. cerevisiae* and *S. pombe* since this fission yeast species can barely use them as the sole carbon source. For ethanol, this phenotype is likely due to the absence of key enzymes in the glyoxylate cycle, which are required to synthesize organic compounds with more than two carbon atoms [27,28]. In the case of glycerol, the addition of minimal amounts of glucose or ethanol to a glycerol-containing medium can revert this phenotype, suggesting that glycerol assimilation in this organism is regulated by additional carbon sources [29].

Macroautophagy/autophagy is a crucial physiological response in eukaryotes induced during nutrient starvation in which distinct cellular components are degraded to basic macromolecules and returned to the cytoplasm for reuse [30]. The autophagic machinery is strongly conserved evolutionarily and involves several "Atg" proteins that act hierarchically [31]. The conserved serine/threonine kinase Atg1, orthologous to mammalian ULK1, is the most upstream component of this pathway [32]. In *S. cerevisiae*, Atg1 kinase activity is controlled by the scaffold proteins Atg13 and Atg17, which allow Atg1 autophosphorylation and activation [33,34]. Once assembled, the Atg1 complex triggers the formation of autophagosomes that eventually fuse with the vacuole to degrade their cargo. The AMPK, target of rapamycin complex 1 (TORC1), cAMP-PKA, and Sch9 signaling pathways convey the nutritional status of the cell to the autophagy machinery in budding yeast. Activation of AMPK

Snf1 during glucose starvation inhibits TORC1 signaling by forming Kog1/RPTOR-bodies [35]. In a nutrient-rich medium, where AMPK activity is low, active TORC1 inhibits Atg1 kinase and autophagy by directly phosphorylating Atg13 [36,37], although Atg1, Atg2, Atg9, and Atg29 have also been identified as direct TORC1 targets [38]. Thus, like in mammalian cells, TORC1 may influence Atg1-Atg13 activity by phosphorylating both complex members [39], whereas PKA and Sch9 cooperate with TORC1 in the negative regulation of autophagy [40].

Mitochondrial respiration has been shown to be required for autophagy induction during amino acid and glucose starvation in *S. cerevisiae* [41,42]. Specifically, active PKA inhibits Atg1-Atg13 phagophore assembly site (PAS) localization and negatively regulates autophagy during amino acid starvation when respiration is blocked. In glucose-starved growth conditions, a mitochondrial signaling hub composed of the DNA damage response pathway component Mec1, Snf1, Atg1, and Atg13, positively regulates autophagy by enhancing the assembly of the Atg1-Atg13-Atg17 complex. Significantly, if mitochondrial respiration is impaired in the absence of glucose, Mec1 is not activated correctly, thus inhibiting Atg1-Atg13 interaction and the autophagic response [42]. Besides, the Mec1-Snf1-Atg1 complex is essential for maintaining mitochondrial respiration [42]. In this regard, the release of serine during autophagy, which is necessary for the stimulation of mitochondrial translation initiation, has been recently shown to be critical for an adequate adaptation of *S. cerevisiae* cells to a respiratory metabolism [43]. However, it is worth noting that autophagy induction upon glucose starvation is a controversial subject in budding yeast since several studies suggest that this stimulus is rather an inhibitor than an inducer of this process [44,45].

Although *S. cerevisiae* and *S. pombe* share many components in the autophagy machinery, their functional organization differs in many aspects. For instance, fission yeast Atg1 kinase activity depends exclusively on Atg11, while Atg13 seems dispensable [46].

Recent work has revealed that TORC1 and TORC2 signaling act in a concerted fashion to negatively regulate the onset of fission yeast autophagy under nutrient-rich conditions [47]. In addition, the SAPK pathway MAPK Sty1, but not the transcription factor Atf1, is important for the enhanced transcription of several *atg* genes to positively modulate autophagy induction [47]. Notwithstanding autophagy during carbon starvation has been extensively studied in budding yeast, very little is known about how the evolutionary distant fission yeast orchestrates autophagy during glucose scarcity. Whereas earlier work showed that autophagy is completely blocked in *S. pombe* upon glucose starvation [48], recent evidence suggests that autophagy can proceed when fission yeasts cells grow in a low glucose medium [47].

In this work, we have exhaustively analyzed the consequences of glucose scarcity in autophagy induction in fission yeast and the nature of the signaling pathways that convey this nutritional cue to the autophagy machinery. We show that mitochondrial respiration is critical for glucose-dependent induction of autophagy during the transition from fermentative to a respiratory metabolism upon glucose limitation or starvation. cAMP-PKA signaling represses this process in the presence of glucose by downregulating the transcription factor Rst2, which elicits the expression of specific respiratory metabolism genes for the induction of autophagy during reduced glucose availability. Moreover, the SAPK MAPK Sty1 crosstalks with PKA-Rst2 signaling by two alternative mechanisms, involving its downstream effector Atf1 and the *in vivo* phosphorylation of Rst2, to positively regulate the transcriptional induction of autophagy upon glucose limitation.

Results

Autophagy is induced in S. pombe *in response to limited glucose availability.*

S. pombe undergoes a strong autophagic response during nitrogen starvation [49,50]. Indeed, the transfer of exponentially growing fission yeast cells expressing an N-terminally tagged CFP-Atg8 fusion [50] from minimal medium EMM2 to a similar medium lacking a nitrogen source (EMM2-N2) was accompanied by a relatively brief appearance of specific CFP-Atg8 puncta within the cell cytoplasm of nitrogen-depleted cells (Fig. S1A). Western blot analysis using the CFP-Atg8 fusion protein processing assay revealed a progressive increase of a free protease-resistant CFP moiety indicative of autophagic delivery to the vacuole and subsequent proteolysis of Atg8 (Fig. S1B). Contrariwise, and as initially described [49], glucose starvation-induced by transfer of exponentially growing fission yeast cells from EMM2 with 7% glucose to a glucose-free medium osmotically equilibrated with 3% of the respirable carbon source glycerol did not result in the appearance of CFP-Atg8 puncta and/or proteolysis (Figure 1A-C; Fig. S1A and S1B). Importantly, cell viability was not significantly affected after the transfer of the cells to glycerol medium (Fig. S1C and S1D), excluding the possibility that cell death is responsible for the lack of autophagy induction during glucose-starvation. However, it has been recently shown that the autophagy flux is activated when *S. pombe* cells are transferred from a glucose-rich medium to a medium supplemented with limited sugar concentrations [47]. Nevertheless, this response's precise nature and mechanisms are currently unknown. To explore this issue, we started by precisely determining the physiological range of limited glucose concentrations that allow the induction of autophagy in fission yeast. As shown in Figure 1A and B, CFP-Atg8 puncta were hardly detected in wild-type cells after 4 h of incubation in EMM2 with glycerol plus 0.01% glucose, but their number increased significantly in medium with 0.02% glucose and reached a maximum in 0.04% glucose. The percentage of cells with puncta declined progressively when incubated in media with 0.08-0.16% glucose and was negligible in the presence of 0.2% of carbon source (Figure 1A and B). Accordingly, a gradual increase in the amount of the protease-resistant CFP tag was detected in extracts from wild-

type cells after 5 and 7 h of incubation in medium supplemented with 0.02, 0.04, or 0.08% glucose (Figure 1C). CFP-Atg8 cleavage was highest during incubation with 0.04-0.08% glucose, slowly declined in 0.12 and 0.16% and was virtually undetectable in the presence of 0.2% glucose (Figure 1C). Therefore, induction of an autophagic response in *S. pombe* during glucose limitation occurs within a specific range of carbon source concentrations. The induction of autophagy occurred similarly when wild-type cells were shifted to EMM2 with 0.5% ethanol plus 3% glycerol (Fig. S1E), a medium in which fission yeast cells can grow because ethanol regulates glycerol assimilation [51]. Interestingly, CFP-Atg8 cleavage was slightly but reproducibly reduced when cells were transferred to EMM2 with 0.04% glucose plus sorbitol (non-respirable) instead of glycerol (Fig. S1F).

The conserved serine/threonine kinase Atg1/ULK1 is a target of several signaling cascades and a pivotal regulator of autophagy induction in eukaryotes, including fission yeast [52,53]. Atg1 activation in fission yeast occurs through a cis-autophosphorylation event mediated by the scaffold protein Atg11 and independently of Atg13 function [46,53]. Similar to nitrogen starvation [50], CFP-Atg8 puncta were present during growth under glucose-limiting conditions in fission yeast mutants in the autophagy initiation machinery components *atg1*Δ and *atg11*Δ, and absent in mutants in the Atg8 conjugation system *atg4*Δ and *atg5*Δ (Figure 1D and E), suggesting that they correspond to the PAS. CFP-Atg8 proteolysis under glucose-limiting conditions was entirely abolished in *atg1*Δ, *atg11*Δ, *atg4*Δ, and *atg5*Δ cells (Figure 1F), confirming the critical role of Atg1 function during autophagy initiation under this specific stimulus. The group of Hidalgo *et al.* has recently described that the two fission yeast TOR complexes TORC1 and TORC2 are negative regulators of autophagy upon nutrient depletion, including glucose [47]. TORC1/2 kinase inhibition elicits Atg1 dephosphorylation in response to nitrogen starvation, resulting in increased electrophoretic mobility that is employed to monitor autophagy onset [47,49]. The electrophoretic mobility of a genomic Atg1-

HA fusion decreased slightly in wild-type cells incubated for 1 h with modified EMM2 with 0.04% glucose, but it was followed by a progressive increase in protein levels and the appearance of faster mobility forms after 3 and 5 h of incubation (Figure 1G). Conversely, increased electrophoretic mobility of the Atg1-HA fusion was not observed during glucose starvation in the presence of glycerol (Figure 1G). Thus, the lack of induction of autophagy in *S. pombe* during glucose starvation, as opposed to glucose limitation, might result from an improper regulation of Atg1 kinase activity.

Mitochondrial respiration is critical for glucose-dependent induction of autophagy.

A threshold in glucose concentration $\leq$ 0.1% governs respiration-dependency of *S. pombe* proliferation [54]. Indeed, fission yeast wild-type cells are able to divide and proliferate in medium with 2% glucose supplemented with 4.4 μM of antimycin A (AA), an inhibitor of ETC Complex III/IV responsible for mitochondrial respiration. On the other hand, AA treatment completely abolishes cellular proliferation when glucose concentrations are lower than 0.1% (Figure 2A) [54]. Together with the above results, these precedents suggest that active respiratory metabolism may be required for full induction of the autophagic response upon glucose limitation. Accordingly, both CFP-Atg8 puncta and proteolysis were completely absent in wild type incubated with 0.04% glucose plus glycerol in the presence of AA (Figure 2B and 2C). Autophagy was not inhibited by AA treatment when wild-type cells were subjected to nitrogen starvation (Fig. S2A and S2B). Remarkably, the Atg1-HA fusion was not dephosphorylated in wild-type cells upon glucose limitation in the presence of AA (Figure 2D) but instead remained unchanged as in glucose-starved cells (Figure 1G). These results support that induction of autophagy under limited glucose concentrations in *S. pombe* specifically relies on mitochondrial respiration.

The above findings prompted us to explore the biological relevance of other ETC components besides complex III/IV during autophagy upon glucose limitation. As seen in Figure 2E, treatment of wild-type cells with rotenone (complex I inhibitor), 2-thenoyltrifluoroacetone (TTFA; complex II inhibitor), and the proton pump inhibitor N,N-dicyclohexylcarbodiimide (DCCD) [55], caused a significant reduction in the autophagic flux in cells transferred to 0.04% glucose plus glycerol as compared to untreated cells. Contrariwise, oligomycin (complex V ATP synthase inhibitor) did not inhibit the autophagic flux, although all the drugs inhibited proliferation of wild-type cells in 0.04% Glu plus 3% Gly solid media without affecting growth in 2% Glu (Fig. S2C). We further investigated the possible role of representative mitochondrial gene products (important for the proper function of ETC complexes) during autophagic induction in response to reduced glucose availability. These included *nde1*$^{+}$ (external mitochondrial NADH dehydrogenase (ubiquinone); complex I), *rip1*$^{+}$ and *qcr2*$^{+}$ (ubiquinol-cytochrome-c reductase complex core protein; complex III), and *atp11*$^{+}$ (F1-FO chaperone component of ATP synthase; complex V) [56]. Specific deletion of complex III genes *rip1*$^{+}$ and *qcr2*$^{+}$ blocked the autophagic process, whereas deletion of *atp11*$^{+}$ caused a significant reduction in the autophagic flux in response to glucose limitation (Figure 2F). Interestingly, cells lacking *rip1*Δ and *qcr2*Δ consumed ~10-fold less the amount of oxygen of wild-type cells, whereas in the *nde1*Δ and *atp11*Δ mutants this reduction was less severe (~2.5-fold) (Figure 2G). These results suggest that the deleted genes in complexes I and V do not completely block their function, probably due to the existence of some functional redundancy with other complexes subunits. This reduced respiratory activity might be enough to favour the onset of autophagy, but insufficient to promote cellular growth, as *nde1*Δ and *atp11*Δ cells are unable to proliferate in 0.04% Glu plus 3% Gly solid plates (Fig. S2D). We conclude that, in fission yeast, induction of autophagy upon glucose-limitation strongly relies on an entirely functional mitochondrial ETC.

Mitochondrial respiration is also necessary to induce autophagy upon glucose limitation in the budding yeast *S. cerevisiae* [42,52]. A module composed of the AMPK Snf1, the DNA damage response pathway component Mec1/ATR, Atg1, and Atg13, is recruited to the mitochondria to initiate autophagy by a mechanism that relies on Atg11, which facilitates the interaction between Snf1 and Atg1 [42,57]. However, deletion of the respective fission yeast AMPK and Mec1 orthologs *ssp2*$^{+}$ [12] and *rad3*$^{+}$ [58], was not detrimental to the induction of autophagy during glucose limitation (Figure 2H), suggesting that the mechanisms that regulate autophagy under this specific stimulus have evolved differently in both yeast species. The Snf1-Mec1-Atg1 module is also essential in budding yeast to maintain mitochondrial respiration [42]. While Ssp2-deleted cells are respiration defective and unable to assimilate glycerol [12], *rad3*Δ, *atg1*Δ, and a*tg11*Δ mutants grew normally with this carbon source (Figure 2I), indicating that autophagy might not be involved in the regulation of mitochondrial function in fission yeast.

cAMP-PKA signaling represses* S. pombe *autophagy flux during the transition from fermentative to a respiratory metabolism.

Glucose detection in *S. pombe* occurs chiefly through a cAMP-PKA signaling pathway that shares many features with mammalian systems, starting with extracellular sensing by the G-protein coupled receptor Git3 (Figure 3A) [20]. The signal is then transmitted to a membrane-bound adenylate cyclase Cyr1 through a heterotrimeric G protein composed of Gpa2/Git8 (α), Git5 (β), and Git11 (γ) subunits [20]. This results in Cyr1 activation and increased intracellular levels of cAMP, which in turn prompt the activation of Pka1 catalytic subunit through its dissociation from the regulatory subunit Cgs1 (Figure 3A) [20]. In sharp contrast to wild type, we observed that glucose starvation in the presence of glycerol elicited the autophagic flux in mutants lacking core components of the cAMP-PKA pathway, including *git3*Δ, *gpa2*Δ*, cyr1*Δ*,*

and *pka1*Δ, as evidenced by the appearance of CFP-Atg8 puncta and proteolysis (Figure 3B-D). Puncta were even detected in a small fraction of cells from the above mutants during growth in glucose-rich medium (Figure 3B, 0 h). Induction of autophagy during glucose starvation was also observed in cells of a thermosensitive allele of the PDPK1/PDK1 (3-phosphoinositide dependent protein kinase 1) ortholog *ksg1-208*, which is responsible for the activation loop phosphorylation of Pka1 (Fig. S3A) [59], or in those expressing a Pka1 phospho-mutant in the specific Ksg1-dependent phosphorylation site ($Pka1^{T356A}$) (Fig. S3B) [60]. Further, in glucose-starved *pka1*Δ cells, the Atg1-HA fusion underwent increased mobility after 3 to 5 h of incubation (Figure 3E), which was reminiscent of that shown by wild-type cells upon glucose limitation (Figure 1G).

CFP-Atg8 proteolysis was significantly accelerated in Pka1-deleted cells during unperturbed growth curve in glucose-rich medium compared to wild-type cells (Fig. S3C) or when transferred to minimal medium with 0.04% glucose plus glycerol (Figure 3F). The dynamics of the autophagic flux were nevertheless identical in wild-type and *pka1*Δ cells starved from nitrogen (Fig. S3D). Most importantly, constitutive activation of cAMP-PKA signaling, achieved in a mutant strain lacking the Pka1 regulatory subunit Cgs1, resulted in a block in CFP-Atg8 proteolysis upon glucose limitation (Figure 3G). Therefore, fission yeast cAMP-PKA dependent signaling represses autophagy under glucose-limiting conditions that induce a respiratory metabolism. Similar to glucose limitation, CFP-Atg8 proteolysis in glucose-starved *pka1*Δ cells was specifically abrogated through inhibition of ETC complexes II, III and V functions in the presence of TTFA, AA, oligomycin and DCCD, respectively (Figure 3H; Fig. S3E) or in double deleted mutants with the complex I gene $nde1^{+}$, complex III genes $rip1^{+}$ and $qcr2^{+}$ and complex V gene $atp11^{+}$ (Fig. S3F). Thus, relief of cAMP- and PKA-dependent inhibition of mitochondrial respiration is critical for inducing autophagy under the above conditions. Moreover, simultaneous deletion of $ssp2^{+}$ did not impair the induction of

autophagy in *pka1*Δ cells starved from glucose in the presence of glycerol (Figure 3I), further supporting that AMPK is not involved in this specific response in fission yeast.

Pre-incubation of *S. pombe* wild-type cells in medium with low-glucose concentrations (0.08%) significantly extends their chronological lifespan upon glucose starvation as compared to cells directly starved from the carbon source (Figure 3J) [61]. The cAMP-PKA pathway is a major regulator of *S. pombe* aging in response to glucose [62,63]. Indeed, the increased chronological life span of *pka1*Δ cells during glucose starvation was similar to that of wild-type cells pre-incubated with 0.08% glucose and was further enhanced by incubation in a low-glucose medium (Figure 3J). Compared to wild type, we noted that chronological life span was strongly reduced in glucose-starved cells of a fission yeast mutant lacking kinase Atg1 with or without pre-incubation in a low glucose medium (Figure 3J). Therefore, like in budding yeast [64], autophagy extends *S. pombe* lifespan during low glucose concentrations growth. Importantly, simultaneous deletion of $atg1^{+}$ significantly reduced the longevity of *pka1*Δ cells during glucose starvation under both conditions (Figure 3J), suggesting that in this organism, the pro-aging effect of glucose and cAMP-PKA signaling is exerted, at least in part, through the inhibition of autophagy.

Pka1 downstream transcription factor Rst2 positively regulates respiration-dependent autophagy in* S. pombe *in response to glucose limitation or starvation.

The transcription factor Rst2, a key effector of the cAMP-PKA pathway in *S. pombe*, becomes phosphorylated by Pka1 at multiple residues to promote its nuclear exclusion and inactivation (Figure 3A) [55,60]. Conversely, in the absence of glucose, Rst2 specifically activates the expression of genes involved in several aspects of the fission yeast life cycle, including sexual differentiation, gluconeogenesis, and growth adaptation to non-fermentable

carbon sources (Figure 3A) [17,18]. Compared to wild type, the number of cells with CFP-Atg8 puncta and its subsequent cleavage were partially but significantly reduced in *rst2*Δ cells when changed to 0.04% glucose plus glycerol medium (Figure 4A and B). Moreover, in *pka1*Δ *rst2*Δ cells subjected to glucose starvation, the accumulation of CFP-Atg8 puncta and the autophagic flux were strongly suppressed compared to *pka1*Δ cells (Figure 4C and D). Accordingly, cells expressing a version of Rst2 lacking Pka1 inhibitory phosphorylation sites (Rst2.M3) [60], showed a similar autophagic response to *pka1*Δ cells during glucose starvation (Figure 4E). However, autophagy in glucose-starved *rst2.M3* cells was strongly alleviated in the *rst2.M3 cgs1*Δ double mutant with constitutive Pka1 activity (Figure 4F). Hence, in *S. pombe,* cAMP-PKA signaling may negatively regulate respiration-induced autophagy in response to glucose limitation or starvation both in an Rst2-dependent and -independent fashion.

The SAPK pathway participates with cAMP-PKA signaling during the transcriptional control of respiration-dependent autophagy upon glucose limitation or starvation.

The SAPK pathway and its core element, the MAPK/p38 ortholog MAPK Sty1, play a critical role in *S. pombe* by modulating the cell cycle and the general adaptive response to environmental cues, including changes in the availability of nitrogen and glucose [65]. During stress, activated cytoplasmic Sty1 translocates to the cell nucleus and phosphorylates the bZIP domain transcription factor Atf1 to induce the expression of a set of the CESR genes [66,67]. These include, among many others, genes like *fbp1*$^{+}$ (fructose-1,6-bisphosphatase Fbp1) or *ctt1*$^{+}$ (catalase), whose respective protein products are required for the assimilation of non-fermentable carbon sources and the attenuation of the ensuing endogenous oxidative stress that occurs in glucose-starved growth conditions [19,66]. Previous observations that both the cAMP-PKA and SAPK pathways functionally crosstalk *in vivo* [68,69], prompted us to explore

the possible role of the SAPK pathway during autophagic induction in response to glucose limitation and/or starvation. Either *sty1*$^{+}$ or *atf1*$^{+}$ deletion induced a mild but significant decrease in CFP-Atg8 proteolysis compared to wild-type cells when grown medium supplemented with 0.04% glucose plus glycerol (Figure 4G). Remarkably, the simultaneous absence of Sty1 or Atf1 in glucose-starved *pka1*Δ cells completely abolished the autophagic flux in the presence of glycerol (Figure 4H). Thus, in fission yeast, respiration-dependent induction of autophagy in response to limited glucose availability or glucose starvation is exerted in part at a transcriptional level by the cAMP-PKA and SAPK signaling pathways through Rst2 and Atf1, respectively.

To identify common gene targets regulated by the Pka1-Rst2 and Sty1-Atf1 transcriptional branches involved in the glucose-dependent induction of autophagy at a global scale, we used DNA microarrays and comparatively measured the gene expression profile in wild-type, *pka1*Δ, *pka1*Δ *rst2*Δ, and *pka1*Δ *atf1*Δ cells growing exponentially in glucose-rich medium. As described in [70], and compared to wild type, *pka1*$^{+}$ deletion led to significant changes in gene expression involving approximately 21% of the total fission yeast genes (1106/5130) ($p<0.05$; FDR<0.05; Log2FC value ≥ 3), with 512 and 594 genes induced and repressed, respectively (Figure 5A; Table S3). The expression levels of a high number of the genes induced in *pka1*Δ cells (336 out of 512 genes; ~65%) were significantly reduced in the *pka1*Δ *rst2*Δ double mutant background. Among the upregulated Rst2-dependent genes are *fbp1*$^{+}$ and *ste11*$^{+}$ (DNA-binding transcription factor Ste11), whose increased expression in the absence of Pka1 function has been previously shown to depend on Rst2 transcriptional activity [71,72], as well as several Ste11-dependent genes involved in various aspects of sexual differentiation process (like *ste7*$^{+}$, *ste6*$^{+}$, *spk1*$^{+}$, *mei2*$^{+}$) (Table S3) [73], thus validating the data obtained with the microarray experiments. Similarly, simultaneous deletion of *rst2*$^{+}$ attenuated the expression of ~50% of the downregulated genes present in *pka1*Δ cells (304 out of 594

genes) (Table S3). Hence, transcriptional regulation by the cAMP-PKA pathway in *S. pombe* relies heavily on Rst2 function.

Comparative microarray analysis of glucose-growing *pka1*Δ vs. *pka1*Δ *atf1*Δ cells showed that ~33% of the upregulated genes in *pka1*Δ cells (169 out of 512 genes) were significantly reduced in *pka1*Δ *atf1*Δ cells (Figure 5A; Table S3). Remarkably, most of these putative Atf1-dependent genes (~86%; 145/169 genes) are present within the 336 Rst2-dependent genes induced in *pka1*Δ cells (Figure 5A; Table S3). Therefore, both Rst2 and Atf1 are responsible for the enhanced expression of a numerous set of genes in the absence of cAMP-Pka1 function during glucose-limited or glucose-starved growth conditions. Next, we performed a functional categorization of the 145 putative Atf1- and Rst2-dependent genes by GO enrichment analysis. Genes involved in the regulation of glycerol metabolism (GO:0006071), positive regulation of pheromone response MAPK cascade (GO:0062038), and cellular response to reactive oxygen species (GO:0034614) were among the most enriched categories (25.1-fold, 22.1-fold, and 11.7-fold enrichment, respectively) (Figure 5B; full data are shown in Table S3). Other relevant categories included carbohydrate metabolic process (GO:0005975) and regulation of conjugation with cellular fusion (GO:0031139) with a 6.2- and 5.1-fold enrichment, respectively (Figure 5B; Table S3). The GO-enriched genes involved in glycerol metabolism were of particular interest and included *gld1*$^{+}$ (mitochondrial glycerol dehydrogenase Gld1), *dak1*$^{+}$ (dihydroxyacetone kinase Dak1) and *dak2*$^{+}$, *gpd1*$^{+}$ (glycerol-3-phosphate dehydrogenase Gpd1), and *gut2*$^{+}$ (glycerol-3-phosphate dehydrogenase Gut2) (Figure 5C). In fission yeast, Gld1 is essential for glycerol assimilation by catalyzing its oxidation to dihydroxyacetone (DHA), which is subsequently phosphorylated to dihydroxyacetone phosphate (DHAP) by the redundant kinases Dak1 and Dak2, and isomerized to glyceraldehyde-3-phosphate to enter into the glycolytic flux (Figure 5C) [29,51,74]. Gut2 and Gpd1 are involved in converting DHAP to glycerol phosphate and vice-versa (Figure 5C)

[74]. In wild-type cells, expression of the *gld1*$^+$, *dak1*$^+$, and *dak2*$^+$ genes is repressed in high glucose concentrations and becomes strongly induced, particularly that of *gld1*$^+$, during glucose starvation [29]. qPCR analysis confirmed that *pka1*$^+$ deletion resulted in significantly increased expression levels of this gene cluster relative to wild-type cells, ranging from the sharp fold increase observed in *gld1*$^+$, *dak1*$^+$, and *dak2*$^+$ genes to lower values in *gut2*$^+$and *gpd1*$^+$genes (Figure 5D). As expected, we confirmed that, in contrast to wild-type, *gpa2*Δ, *cyr1*Δ and *pka1*Δ, and to a lesser extent, *git3*Δ cells, were able to proliferate in glucose-free glycerol-containing medium (Fig. S4A). Simultaneous deletion of *rst2*$^+$ or *atf1*$^+$ in *pka1*Δ cells markedly reduced the mRNA expression levels of these genes to those present in wild-type cells (Figure 5D), confirming that gene de-repression in the absence of Pka1 function is dependent on both transcription factors. Accordingly, the strong expression of a genomic Gld1-HA fusion observed in *pka1*Δ cells during growth in glucose-rich medium and in the absence of this carbon source was largely dependent on Rst2 and/or Atf1 (Figure 5E). Similarly, either *atf1*$^+$ or *rst2*$^+$ deletion strongly reduced the expression of *gld1*$^+$, *dak1*$^+$, and *dak2*$^+$ genes and Gld1-HA levels in wild-type cells upon glucose limitation for 2 h (Figure 5E and F). In contrast, the increased expression of *gut2*$^+$ and *gpd1*$^+$, precluded in *atf1*Δ cells, was unaffected by *rst2*$^+$ deletion (Figure 5F).

Most importantly, we found that single deletion of *gld1*$^+$ or double deletion of *dak1*$^+$ and *dak2*$^+$ genes slowed down autophagy during glucose limitation compared to wild-type cells, and strongly attenuated this process upon glucose starvation in *pka1*Δ cells (Figure 5G and H). Moreover, the onset of autophagy was blocked when glucose-starved *pka1*Δ cells were incubated with the non-respirable carbon source sorbitol (Fig. S4B), and despite that Gld1, Dak1 and Dak2 are de-repressed in the presence of glucose (Figure 5D and E). Contrary to the *gld1*Δ and *dak1*Δ *dak2*Δ mutant backgrounds, the autophagic flux remained unchanged during glucose limitation and glucose starvation in *pka1*Δ cells lacking either *gut2*$^+$, *gpd1*$^+$, or gene

products from different GO-enriched groups like the gluconeogenic fructose-1,6-bisphosphatase gene *fbp1*$^{+}$ (Fig. S4C and S4D). Hence, in fission yeast, the respective inhibition and activation of cAMP-PKA and Sty1 signaling, and the ensuing enhanced expression of glycerol assimilatory genes *gld1*$^{+}$, *dak1*$^{+}$, and *dak2*$^{+}$ by Rst2 and Atf1 transcription factors play a significant role during respiration-dependent induction of autophagy.

In vivo phosphorylation by Sty1 at S292 positively modulates Rst2 transcriptional activity and the induction of autophagy during respiration in response to glucose limitation or starvation.

Rst2 undergoes a phosphorylation-dependent mobility shift when *S. pombe* cells are starved from glucose [18,55]. As expected, a genomic Rst2-3HA fusion, which migrates as a doublet in glucose-growing wild-type cells lacking the vacuolar serine protease Isp6 to minimize Rst2 degradation, underwent a pronounced mobility shift and resolved as a single phosphorylated band when its expression levels increased during glucose limitation or starvation (Figure 6A and B). Pka1 absence did not affect Rst2-HA mobility shift during glucose starvation [18,55], but it increased its overall expression levels (Figure 6B), suggesting that activated Rst2 might favor its own expression. Importantly, Sty1 absence, but not that of Atf1, strongly impaired Rst2-HA mobility shift in wild-type and *pka1*Δ cells during both glucose limitation and starvation (Figure 6A and B), indicating that Rst2 might be targeted and phosphorylated by the MAPK *in vivo*. Rst2 amino acid sequence has ten putative MAPK phosphorylation sites (T39, S245, S292, S354, S358, S398, S405, S410, S422, and S438), two of which, S245 and S292 (consensus sequence: -PXS/TP-), have been shown to become phosphorylated *in vivo* in global phosphoproteomics studies (Figure 6C) [75-77]. We obtained a rabbit polyclonal phospho-antibody that recognizes Rst2 phosphorylation at S292 *in vivo*. This antibody is specific for this modified residue since S292 phosphorylation was absent in

452 *rst2*Δ and *rst2*^{S292A} mutants (Fig. S5A and S5B) or in wild-type cells after phosphatase treatment
453 without a phosphatase specific inhibitor (Fig. S5C). *In vivo* phosphorylation of Rst2 at S292
454 was minimal in wild-type cells during vegetative growth in glucose-rich medium but increased
455 significantly in response to glucose limitation (Figure 6D; Fig. S5A). The highly unstable nature
456 of the Rst2-HA fusion during purification under native conditions prevented us from exploring
457 its *in vivo* association with Sty1. Nevertheless, compared to wild type, Rst2 phosphorylation at
458 S292 was totally absent in cells lacking Sty1 during unperturbed growth and glucose limitation
459 (Figure 6D), strongly suggesting that Sty1 indeed phosphorylates this site *in vivo*.
460 Similar to *pka1*Δ *rst2*Δ cells, increased mRNA expression levels of the glycerol
461 metabolic genes *gld1*$^{+}$, *dak1*$^{+,}$ and *dak2*$^{+}$ were strongly and significantly reduced in *pka1*Δ cells
462 expressing the phosphonull *rst2*^{S292A} mutant allele (Figure 6E). Therefore, *in vivo* Sty1-
463 dependent phosphorylation at S292 may enhance Rst2 transcriptional activity in response to
464 limited glucose availability. However, the overall significance of Sty1-dependent
465 phosphorylation at S292 of Rst2 was mild since, in contrast to *rst2*$^{+}$ deletion, cells expressing
466 Rst2^{S292A} were able to grow in the presence of 3% glycerol under respiratory conditions (Fig.
467 S5D). Also, Rst2 mobility shift during glucose limitation was not impaired by the S292A
468 mutation (Fig. S5B), suggesting that it might be phosphorylated by Sty1 *in vivo* at additional
469 serine and/or threonine residues. Nevertheless, we observed that the number of cells with CFP-
470 Atg8 puncta and its proteolysis declined significantly in cells expressing the Rst2^{S292A} mutant
471 version with respect to wild type after a change to a medium with 0.04% glucose plus glycerol
472 (Figure 6F), and were further reduced in glucose-starved *pka1*Δ cells (Figure 6G). Of note,
473 CFP-Atg8 proteolysis in cells expressing a version of Rst2 mutated at the second perfect MAPK
474 phospho-site S245 (Rst2^{S245A}; Figure 6C) was also similar to the control cells grown under
475 glucose-limiting conditions (Fig. S5E). As a whole, these findings indicate that *in vivo*

phosphorylation of Rst2 at S292 by Sty1 has a positive effect during the respiration-dependent transcriptional induction of autophagy upon glucose limitation or starvation.

Discussion

In this work, we have explored the regulatory mechanisms that induce autophagy upon glucose limitation and starvation in the fission yeast *S. pombe* and demonstrated that mitochondrial respiration is essential for activating this adaptive physiological response. First, the glucose concentrations in the growth medium that render cells permissive to induce autophagy lay within the range that governs respiratory metabolism in fission yeast (Figure 1) [54]. Second, ETC complexes I, II, III and V inhibition with rotenone, TTFA, AA and DCCD, or gene deletion of complex III and V components (Rip1, Qcr2, Atp11) caused a strong reduction in the autophagic flux under limited glucose concentrations (Figure 2). Mitochondrial respiration is also required for autophagy in *S. cerevisiae* in response to glucose limitation [42]. However, our data support that the specific mechanisms that link mitochondrial respiration to autophagy have likely diverged in both yeast species. Accordingly, the autophagic flux was not compromised upon glucose limitation in fission yeast mutants deleted in the DNA damage response pathway Mec1/ATR ortholog Rad3 or in cells lacking AMPK Ssp2 (Figure 2H). The null effect of *ssp2*$^{+}$ deletion on the autophagic flux was somehow unexpected, considering its role as a negative regulator of TORC1 complex function [78], which in turn downregulates autophagy upon glucose depletion [47]. Also, in budding yeast, Atg11 is exclusively required for the induction of bulk autophagy upon glucose limitation [57], while in fission yeast, Atg11 plays a general role to induce autophagy in the absence of both nitrogen and glucose (Figure 1) [53]. Finally, in budding yeast, Mec1, Atg1, and Atg11 are required to maintain mitochondrial respiration during glucose limitation [42]. In contrast, the corresponding fission yeast orthologs

500 are not (Figure 2I), suggesting that in *S. pombe,* autophagy is not likely involved in regulating
501 mitochondrial function.

502 *S. pombe* cells cannot induce autophagy upon glucose starvation (Figure 1) [47,49].
503 Although it has been described that *S. cerevisiae* induces a strong autophagic response when
504 starved from glucose [42,79], there is some controversy on this issue since other works showed
505 that glucose starvation instead inhibits autophagy in this yeast species [44]. Inactivation of
506 cAMP-PKA signaling in *S. cerevisiae* cells expressing an analog-sensitive Tpk1 allele as the
507 sole source of PKA activity was sufficient to allow the induction of autophagy in glucose-rich
508 medium [80]. Contrariwise, in fission yeast, deletion of Pka1 catalytic subunit *pka1*$^{+}$, which is
509 not lethal, did not prompt autophagy in nutrient-rich conditions (Figure 3). Nevertheless,
510 glucose-starved *pka1*Δ cells induced a strong autophagy response when shifted to a medium
511 with glycerol, a non-fermentable carbon source. In contrast, constitutive Pka1 activation
512 achieved in the absence of its regulatory subunit Cgs1 blocked autophagy during glucose
513 limitation (Figure 3). Hence, in fission yeast, the cAMP-PKA signaling pathway acts as a
514 repressor of autophagy in the presence of glucose, and this regulatory mechanism is likely
515 exerted both at transcriptional and post-transcriptional levels.

516 We found that the cAMP-PKA dependent transcriptional regulation of autophagy is
517 funneled via the Rst2 transcription factor. Rst2 transcriptional activity is inhibited in glucose-
518 growing cells through a Pka1-dependent phosphorylation mechanism and becomes fully
519 operative as Pka1 activity decreases during glucose limitation or starvation [17,55,71].
520 Significantly, *rst2*$^{+}$ deletion reduced the autophagic flux of wild-type and *pka1*Δ cells in
521 response to glucose limitation and blocked it upon starvation (Figure 4). Further, by performing
522 microarray analysis we identified the glycerol metabolism genes *gld1*$^{+}$, *dak1*$^{+}$, and *dak2*$^{+}$ as
523 key Rst2 targets whose expression is necessary for proper induction of respiration-dependent
524 autophagy. Accordingly, their respective deletion mirrored the reduced autophagic flux

prompted by *rst2*$^{+}$ deletion in wild-type and *pka1*Δ cells upon glucose limitation and starvation in the presence of glycerol (Figure 5). In *S. cerevisiae*, glycerol is assimilated through a glycerol 3-phosphate (Gly-3-P) pathway and is degraded during osmotic stress via a DHA pathway catalyzed by the glycerol dehydrogenase Gcy1 and the DHA kinases Dak1 and Dak2 [74]. However, *S. pombe* lacks a Gly-3-P pathway, and therefore the DHA pathway genes encoding glycerol dehydrogenase Gld1 and Dak1/2 are essential in this organism for glycerol assimilation [29]. It was initially shown that Ssp2 target Scr1 represses the expression of *gld1*$^{+}$ in the presence of glucose [29]. In this work, we found that *gld1*$^{+}$ mRNA levels are strongly induced in an Rst2-dependent fashion in wild-type cells upon glucose limitation or in glucose-growing *pka1*Δ cells, suggesting that putative binding of Rst2 to the *gld1*$^{+}$ promoter is favored upon Scr1 absence. Both Rst2 and Scr1 bind the DNA motif 5′-CCCCTC-3′, and it has been described that Rst2 replaces Scr1 at the *fbp1*$^{+}$ promoter upon glucose starvation to induce gene expression [16]. Moreover, genome-wide analysis of carbon catabolite repression in fission yeast suggests that most of the Scr1-repressed genes might be reciprocally activated by Rst2 during glucose starvation in the absence of Scr1 function [17]. Our data support that positive control of *gld1*$^{+}$ expression by Rst2 is dominant over the repressor activity of Scr1 for the induction of autophagy since *ssp2*$^{+}$ deletion, which prevents Scr1 inhibition, did not reduce the autophagic flux in *pka1*Δ cells starved from glucose in the presence of glycerol (Figure 3I). In addition, the induced expression of *dak1*$^{+}$ and *dak2*$^{+}$ genes, which are not repressed by Scr1 [29], is Rst2-dependent (Figure 5F), thus providing an additional layer for the transcriptional regulation of autophagy in the absence of glucose. The intense autophagic flux of glucose-starved cells expressing an Rst2 version insensitive to negative regulation by cAMP-PKA signaling was reduced markedly in cells with constitutive Pka1 activity (Figure 4F), supports that in fission yeast cAMP-PKA signaling may also negatively regulate autophagy post-translationally and in an Rst2-independent fashion. Although currently unknown, this

550 mechanism might involve the Pka1-dependent inhibitory phosphorylation of Atg1 and/or
551 Atg13, as described in *S. cerevisiae* [81-83].

552 In *S. pombe,* the SAPK pathway and its core effector MAPK Sty1 orchestrate cellular
553 responses to environmental changes [65,67,84-86]. During glucose limitation or starvation,
554 Sty1 activation prompts Atf1 phosphorylation and activation, resulting in the enhanced
555 expression of genes that belong to distinct functional categories, including the CESR genes
556 [66]. Additionally, the SAPK pathway becomes constitutively activated in mutants lacking
557 Pka1 activity due to an endogenous metabolic oxidative stress originated by the adaptation to a
558 respiratory metabolism [56,63]. Our comparative microarray studies revealed that the induced
559 expression of a high number of genes (145) in Pka1-less cells is strictly co-dependent on both
560 Rst2 and Atf1 functions. Notably, among this group of genes were *gld1*$^+$, *dak1*$^+$, and *dak2*$^+$,
561 whose expression is necessary for proper induction of autophagy during glucose limitation.
562 Thus, both the Pka1-Rst2 and Sty1-Atf1 signaling pathways converge to up-regulate the
563 expression of specific respiratory metabolism genes for the induction of autophagy upon
564 glucose limitation. It has been recently described that Sty1 activates autophagy during nitrogen
565 depletion through a mechanism that involves the transcriptional upregulation of *atg* genes,
566 including *atg1*$^+$, *atg4*$^+$, *atg6*$^+$, *atg9*$^+$ and *atg22*$^+$, and independently of Atf1 function [47]. These
567 findings, together with the observations presented here, underscore the key role and remarkable
568 functional plasticity of this signaling pathway to regulate fission yeast autophagy in response
569 to nutrient depletion.

570 Another important finding in this work is that Sty1 phosphorylates Rst2 at S292 to
571 enhance its transcriptional activity and the modulation of autophagy in response to glucose
572 depletion (Figure 6). Deletion of *sty1*$^+$, but not that of *atf1*$^+$, strongly impaired the
573 phosphorylation-dependent mobility shift of an Rst2-HA fusion in wild-type and *pka1*Δ cells
574 upon glucose limitation or starvation. Rst2 phosphorylation by Sty1 might enhance its binding

affinity and recruitment to the regulatory sequences in its downstream gene targets, a control that could be fully exerted by the phosphorylation of the remaining MAPK phosphosites within the protein. These pieces of evidence support that the fission yeast SAPK pathway crosstalks with Pka1-Rst2 signaling through the direct phosphorylation of transcription factor Rst2 to positively regulate the transcriptional induction of autophagy upon glucose limitation.

The key findings described here are summarized in a model presented in Figure 7. *S. pombe* cells grow essentially through a fermentative metabolism when high glucose concentrations are available, although mitochondrial respiration is also required for optimal cell proliferation [87]. This metabolic status results in the upregulation of the TOR and cAMP-PKA signaling pathways, which block autophagy onset by inhibiting the activity of Atg1 kinase and Rst2 transcription factor, respectively, while Atg1 might be as well negatively regulated by Pka1. Also, the CR transcriptional repressor Scr1 constitutively blocks transcriptional induction of genes for assimilation of alternative carbon sources (glycerol). Upon glucose limitation or starvation, downregulation of cAMP-PKA signaling and activation of the SAPK MAPK Sty1 elicit Rst2 nuclear translocation and Atf1 activation, respectively, which, together with Sty1-dependent phosphorylation of Rst2 at S292 and AMPK (Ssp2)-mediated nuclear export of Scr1, lead to the specific transcriptional activation of glycerol assimilatory genes (*gld1*$^{+}$, *dak1*$^{+}$, *dak2*$^{+}$), and the establishment of respiratory metabolism. Finally, the absence of TOR and Pka1-dependent inhibition converge post-transcriptionally with ETC mitochondrial respiration complexes through unknown mechanisms to promote full activation of Atg1 kinase and the ensuing induction of autophagy. Our data reveal the existence of a highly sophisticated and multifaceted environmental control of this essential adaptive response.

Materials and Methods

Fission yeast strains, gene disruption and epitope tagging.

The *S. pombe* strains used in this work are listed in Table S1. Several of the deletion strains were obtained from the Bioneer mutant library [88], whereas null mutants in *atg1*$^+$, *pka1*$^+$, *rst2*$^+$, *rad3*$^+$, *qcr2*$^+$, and *rip1*$^+$ genes were obtained by ORF deletion and replacement with G418 (kanR; Calbiochem, 345810), nourseothricin (NAT; Jena Bioscience, AB-102L), or hygromycin B (Roche, 10843555001), cassettes by employing a PCR-mediated strategy [89,90], and the oligonucleotides described in Table S2. Plasmids pFA6a-3HA-kanMX6 (Addgene, 39295; Jurg Bahler) and pFA6a-GFP-kanMX6 (Addgene, 39292; Jurg Bahler) were employed to obtain genomic C-terminally 3HA- and GFP-tagged versions of Rst2, Gld1, and Atg1. Strains expressing different genomic fusions in multiple genetic backgrounds were constructed either by transformation or after random spore analysis of appropriate crosses in sporulation agar (SPA; 55.5 mM glucose, 7.3 mM KH_2PO_4, 1mL/L vitamins [1000x] {4.20 mM pantothenic acid, 81.2 mM nicotinic acid, 55.5 mM inositol, 40.8 μg biotin}, 20 g/L agar) medium [91].

Growth conditions and treatments.

Fission yeast was routinely grown with shaking at 28ºC in rich (YES; 0.6% yeast extract; Gibco, 212720) or minimal (EMM2; 93.5 mM ammonium chloride, 14.7 mM potassium hydrogen phthlate, 15.5 mM Na_2HPO_4 anhydrous, 20 mL/L salt stock [50x] {0.26 M $MgCl_2.6H_2O$, 4.99 mM $CaCl_2.2H_2O$, 0.67 M KCl, 14.1 mM Na_2SO_4}, 1 mL/L vitamins [1000x] {4.20 mM pantothenic acid, 81.2 mM nicotinic acid, 55.5 mM inositol, 40.8 μg biotin}, 0.1 mL/L minerals [10,000x] {80.9 mM boric acid, 23.7 mM $MnSO_4$, 13.9 mM $ZnSO_4.7H_2O$, 7.40 mM $FeCl_2.6H_2O$, 2.47 mM molybdic acid, 6.02 mM KI, 1.60 mM $CuSO_4.5H_2O$, 47.6 mM citric acid}) media with 2% glucose and supplemented with 100 mg/L adenine (Apollo Scientific,

BIA0543), leucine (Sigma-Aldrich, L8912), histidine (Sigma-Aldrich, H8125), or uracil (Sigma-Aldrich, U0750) [92]. Solid medium was made by adding 2% agar (Difco, 214510). In glucose limitation and starvation experiments, cells were grown in EMM2 with 7% glucose (to ensure a full catabolite repression, maintain osmolarity, and to standardize growth conditions) to a final A_{600} of 0.5, recovered by filtration, and resuspended in the same medium lacking glucose and osmotically equilibrated with 3% glycerol, 7% sorbitol, in media with limiting glucose concentrations (0.02 to 0.2%, depending on the experiment) plus equivalent amounts of glycerol. For starvation, medium with 0.5% ethanol plus glycerol was also employed where indicated. In nitrogen starvation experiments, strains growing exponentially in EMM2 with 2% glucose (A_{600} of 0.5), were recovered by filtration and resuspended in the same medium lacking ammonium chloride. In experiments performed with ETC inhibitors, exponentially growing cultures in EMM2 were pre-treated with either 25.6 µg/ml rotenone (Santa Cruz Biotechnology, sc-203242), 0.5 µM AA (Sigma-Aldrich, A8674), 2 mM TTFA (Santa Cruz Biotechnology, sc-251801), 10 µM oligomycin (Sigma-Aldrich, 495455), or 500 µM DCCD (Sigma-Aldrich, D80002) for 1 h, recovered by filtration, and resuspended in the corresponding media with limited amounts of glucose, or lacking glucose or nitrogen source.

Measurement of oxygen consumption.

For oxygen consumption experiments, cells were grown in EMM2 7% Glu to a final A_{600} of 0.4. The measurements were made using an HI7640714 oximeter (Hanna Instruments), and readings were recorded every minute for 15 min, according to the protocol described in [56].

Measurement of chronological lifespan.

650 *S. pombe* wild-type and mutant strains grown in EMM2 with 7% glucose were recovered by
651 filtration, incubated in low-glucose medium (0.08%) for 6 h, and finally resuspended for 7 days
652 in the same medium lacking glucose. Cell viability was measured after this 7-day incubation
653 period by counting the colony-forming units (CFUs) of appropriate dilutions in YES plates
654 incubated for 3 days at 30ºC. It is expressed as the ratio of the number of colonies formed to
655 the total number of cells plated. The averages of three independent experiments ± SD are
656 shown.
657
658 ***Measurement of cell viability.***
659
660 *S. pombe* wild-type cells grown in EMM2 with 7% glucose were recovered by filtration, and
661 resuspended for the times indicated in the same medium lacking glucose and in the presence of
662 3% glycerol. Cell viability was measured by counting the CFU of appropriate dilutions in YES
663 plates incubated for 3 days at 30ºC. It is expressed as percentage of CFU and was calculated as
664 follows: CFU (%)=(CFU number of glycerol-grown cells)/(CFU number of glucose-grown
665 cells)x100. The averages of three independent experiments ± SD are shown.
666
667 ***Rst2 site-directed mutagenesis.***
668
669 To construct the template plasmid pTA-Rst2:HA, the *rst2*$^{+}$ C-terminally HA-tagged ORF plus
670 regulatory sequences, the kanMX6 cassette, and 3' UTR were amplified by PCR using genomic
671 DNA from Rst2-3HA cells as the template and the 5' oligonucleotide Rst2-HA-FWD, which
672 hybridizes −1025 to −1000 bp upstream of the *rst2*$^{+}$ start codon, and the 3' oligonucleotide
673 Rst2-HA-REV, which hybridizes +580 to +605 bp downstream of the *rst2*$^{+}$ stop codon (Table
674 S2). The PCR fragment was cloned into plasmid pCR2.1 using the TOPO TA Cloning Kit

675 (Thermo Fisher Scientific, 451641) and confirmed by sequencing. Plasmids pTA-Rst2^{S292A}-HA
676 and pTA-Rst2^{S245A}-HA, were obtained by one-step site-directed mutagenesis PCR using
677 plasmid pTA-Rst2:HA as a template and the corresponding mutagenic oligonucleotide pairs
678 Rst2-S292A-FWD/Rst2-S292A-REV and Rst2-S245A-FWD/Rst2-S245A-REV (Table S2).
679 The above plasmids were used as PCR templates to obtain the corresponding DNA fragments,
680 which were transformed into wild-type strain MM1. G418-resistant transformants were
681 obtained, and the correct integration of the respective genomic wild-type (Rst2-3HA), and
682 mutated fusions (Rst2^{S292A}-3HA, Rst2^{S245A}-3HA), were verified by both PCR and western blot
683 analysis. The incorporation of the mutagenized residues was confirmed by sequencing.
684
685 ***Microarray experiments and enrichment analysis.***
686
687 Total RNA was extracted from wild-type, *pka1*Δ*, pka1*Δ *rst2*Δ*,* and *pka1*Δ *atf1*Δ strains
688 growing exponentially in glucose-rich medium (two biological replicates were included for
689 each strain genotype) with RNeasy mini kit (Qiagen, 74104), according to the instructions from
690 the manufacturer, and amount and quality of the RNA checked with a Bioanalyzer 2100
691 (Agilent Technologies, United States). cDNA was synthesized from 100 ng of total RNA from
692 each sample using the GeneChip 3′ IVT PLUS Reagent kit (Affymetrix, ThermoFisher
693 Scientific, 902415). The amount and quality of cDNA and cRNA intermediates were checked
694 with Nanodrop 2000 (ThermoFisher Scientific, United States) and Bioanalyzer 2100. Labeled
695 cRNA targets were purified, and 5 µg of fragmented biotinylated cRNA were included in the
696 hybridization mix by using the GeneChip Hybridization, Wash and Stain kit (Affymetrix,
697 ThermoFisher Scientific, 900720), following the recommendations of the manufacturer. The
698 resulting preparations were hybridized to GeneChip Yeast Genome 2.0 Arrays (Affymetrix,
699 ThermoFisher Scientific, 900553), which include 5,021 probe sets as 11 oligonucleotide pairs

corresponding to 5,031 genes present in the *S. pombe* genome. After scanning, microarray data were processed using Affymetrix Expression Command Console (Affymetrix, ThermoFisher Scientific), and all samples passed the quality criteria. Data analysis was performed with RMA (Robust Multiarray Average). The raw intensity values were background corrected, log2 transformed, and quantile normalized to obtain an individual intensity value for each probe set with the Partek Genomics Suite and Partek Pathways software (Partek Incorporated, St. Louis, USA). The full microarray data are available at ArrayExpress (accession number E-MTAB-11624). The proteins encoded by the statistically significant 145 upregulated genes in *pka1*Δ cells, whose expression depends upon both Rst2 and Atf1 transcription factors, were subjected to a GO enrichment analysis. This analysis was performed using the enrichment analysis tool from the PANTHER classification system [93], with respect to the GO biological process as annotated on PomBase [94].

cDNA synthesis and quantitative real-time polymerase chain reaction (qPCR).

Total RNAs were purified from *S. pombe* wild-type and mutant strains as described above using an RNeasy mini kit (Qiagen, 74104), treated with SUPERase RNase Inhibitor (Invitrogen, AM2696), and quantitated using Nanodrop 100 spectrophotometer (Thermo Scientific, United States). Total RNAs (1 μg) were reverse transcribed into cDNA with the iScript cDNA Synthesis Kit (Bio-Rad, 1708891). qPCR were performed using the iTaq Universal SYBR Green Supermix (Bio-Rad, 172-5124) and a CFX96 Real Time PCR system (Bio-Rad, United States). Relative gene expression was quantified based on the $2^{-\Delta\Delta CT}$ method and normalized using 28S mRNA expression in each sample. The list of gene-specific primers for qPCR is indicated in Table S2. Mean relative units $\pm$ SD are shown.

CFP-Atg8 processing assay.

Cell lysates of strains expressing a CFP-Atg8 fusion under the control of the endogenous promoter [50], were prepared by precipitation with trichloroacetic acid (TCA [Sigma, T9159]) as previously described [95]. Proteins were resolved in 12% SDS-PAGE (sodium dodecyl sulfate polyacrylamide gel electrophoresis) gels, transferred to nitrocellulose blotting membranes (Amersham, 10600003) and immunoblotted with a mouse polyclonal anti-GFP antibody (Roche, 11814460001). Rabbit monoclonal anti-PSTAIR (anti-Cdc2; Sigma-Aldrich, 06-923) was used for loading control. Immunoreactive bands were revealed, respectively, with anti-mouse (Abcam, ab205719) and anti-rabbit HRP-conjugated secondary antibodies (Abcam, ab205718) and the ECL system (GE-Healthcare, RPN2106V1).

Detection of Rst2, Atg1 and Gld1 protein levels and in vivo Rst2 phosphorylation at S292.

Cells from yeast cultures were fixed and total protein extracts were prepared by precipitation with TCA as previously described [95]. Proteins were resolved in 8% (Rst2) or 10% (Atg1, Gld1), SDS-PAGE gels and transferred to nitrocellulose blotting membranes (Amersham, 10600003). To detect Rst2 phosphorylation at S292, urea-denatured protein extracts [86], were hybridized with an anti-phospho-polyclonal antibody produced by immunization of rabbits with a synthetic phosphopeptide corresponding to residues surrounding Ser292 of Rst2 (GenScript). Total Rst2-HA, Atg1-HA and Gld1-HA fusions were detected employing a rat monoclonal HRP-conjugated anti-HA antibody (3F10; Roche, 12013819001). Rabbit monoclonal anti-PSTAIR (anti-Cdc2; Sigma-Aldrich, 06-923) was used for loading control. Immunoreactive bands were revealed with anti-rabbit HRP-conjugated secondary antibodies (Abcam, ab205718), and the ECL system (GE-Healthcare, RPN2106V1).

Lambda phosphatase treatment .

In the Rst2 dephosphorylation assay 10 μg of total urea-denatured extracts were treated with 40 U of λ-protein phosphatase (New England Biolabs, P0753S), in the presence/absence of a specific phosphatase inhibitor (5 mM sodium orthovanadate [Sigma-Aldrich, 5.08605) for 50 min at 30°C as described [86]. Protein electrophoresis was performed on 8% SDS-PAGE gels and Rst2-HA total levels and phosphorylation at S292 were detected as indicated above.

Quantification and reproducibility of western blots.

Densitometric quantification of western blot signals as of 16-bit .jpg digital images of blots was performed using Fiji (ImageJ, National Institutes of Health) [96]. The desired bands plus background were drawn as rectangles and a profile plot was obtained for each band (peaks). Percentage of CFP-Atg8 proteolysis was estimated at each time point by determining the signal ratio of the CFP-Atg8 band with respect to the free CFP band, and normalized with anti-Cdc2 (internal loading control). Depending on the experiment, quantification data shown may correspond to representative experiments, or those performed as biological duplicates or triplicates. Mean relative units $\pm$ SD and/or representative results are shown.

Microscopy observations.

Fluorescence images were obtained with a Leica DM4000B microscope equipped with a Leica DC400F camera and processed using IM500 Image Manager software. The percentage of cells

774 with visible CFP-Atg8 puncta was determined at each time point (number of cells ≥300) from
775 at least three independent experiments and represented as mean ± SD.
776
777 ***Statistical analysis.***
778
779 Graphs and statistical analyses were performed with Prism 6.0 (GraphPad Software). Statistical
780 comparison between strains and *P*-values were analyzed by one-way ANOVA. For statistical
781 analysis of the microarray data, an ANOVA test (T-student) was applied with a restrictive
782 threshold at FDR adjusted p-value ≤ 0.05 and FCh≥2.
783
784 **Acknowledgments**

785 The authors want to thank Li Ling Du, Sergio Moreno, and Pilar Pérez for fission yeast strains
786 and plasmids. We would like to thank María José López-Andreo (Molecular Biology
787 Service/ACTI, University of Murcia, Murcia), for her invaluable help with microarray analyses.
788 This research was funded by the Agencia Estatal de Investigación and Ministerio de Ciencia e
789 Innovación, Spain, grant number PID2020-112569GB-I00, and the Fundación Séneca de la
790 Región de Murcia, Spain, grant number 20856/PI/18, and European Regional Development
791 Fund (ERDF), co-funding from the European Union. Armando Jesús Pérez-Díaz and Francisco
792 Prieto-Ruiz are, respectively, Formación de Profesorado Universitario (FPU) PhD fellows from
793 the Universidad de Murcia and Ministerio de Educación y Formación Profesional, Spain.
794
795 **Data and code availability**
796 All images included in the main and supplemental figures are available as Mendeley dataset
797 (doi: 10.17632/rwdbymndmj.2).
798

Disclosure statement

The authors declare neither financial nor non-financial conflict of interest.

ORCID

Armando Jesús Pérez-Díaz https://orcid.org/0000-0002-5494-0087

Beatriz Vázquez-Marín https://orcid.org/0000-0001-5334-2950

Jero Vicente-Soler https://orcid.org/0000-0001-8759-6545

Francisco Prieto-Ruiz https://orcid.org/0000-0003-0698-3952

Teresa Soto https://orcid.org/0000-0003-2965-318X

Alejandro Franco https://orcid.org/0000-0001-7461-3414

José Cansado https://orcid.org/0000-0002-2342-8152

Marisa Madrid https://orcid.org/0000-0002-7970-2587

References

1. Broach JR. Nutritional control of growth and development in yeast. Genetics. 2012; 192(1):73-105.
2. Pfeiffer T, Morley A. An evolutionary perspective on the Crabtree effect. Front Mol Biosci. 2014;1:17.
3. Vemuri GN, Altman E, Sangurdekar DP, et al. Overflow metabolism in *Escherichia coli* during steady-state growth: transcriptional regulation and effect of the redox ratio. Appl Environ Microbiol. 2006;72(5):3653-3661.
4. van Dijken JP, Weusthuis RA, Pronk JT. Kinetics of growth and sugar consumption in yeasts. Antonie Van Leeuwenhoek. 1993;63(3-4):343-52.
5. Vander Heiden MG, Cantley LC, Thompson CB. Understanding the Warburg effect: the metabolic requirements of cell proliferation. Science. 2009;324(5930):1029-1033.
6. Malina C, Yu R, Björkeroth J, et al. Adaptations in metabolism and protein translation give rise to the Crabtree effect in yeast. Proc Natl Acad Sci U S A. 2021;118(51).
7. Gancedo JM. Yeast carbon catabolite repression. Microbiol Mol Biol Rev. 1998; 62(2):334-61.
8. Adnan M, Zheng W, Islam W, et al. Carbon catabolite repression in filamentous fungi. Int J Mol Sci. 2017;19(1):48.
9. Kremling A, Geiselmann J, Ropers D, et al. Understanding carbon catabolite repression in *Escherichia coli* using quantitative models. Trends Microbiol. 2015;23(2):99-109.
10. Romano A, Koczwara JB, Gallelli CA, et al. Fats for thoughts: An update on brain fatty acid metabolism. Int J Biochem Cell Biol. 2017;84:40-45.
11. Tanaka N, Ohuchi N, Mukai Y, et al. Isolation and characterization of an invertase and its repressor genes from *Schizosaccharomyces pombe*. Biochem Biophys Res Commun. 1998;245(1):246-253.

12. Matsuzawa T, Fujita Y, Tohda H, et al. Snf1-like protein kinase Ssp2 regulates glucose derepression in *Schizosaccharomyces pombe*. Eukaryot Cell. 2012;11(2):159-167.
13. Hanyu Y, Imai KK, Kawasaki Y, et al. *Schizosaccharomyces pombe* cell division cycle under limited glucose requires Ssp1 kinase, the putative CaMKK, and Sds23, a PP2A-related phosphatase inhibitor. Genes Cells. 2009;14(5):539-554.
14. Lundin M, Nehlin JO, Ronne H. Importance of a flanking AT-rich region in target site recognition by the GC box-binding zinc finger protein MIG1. Mol Cell Biol. 1994;14(3):1979-1985.
15. Papamichos-Chronakis M, Gligoris T, Tzamarias D. The Snf1 kinase controls glucose repression in yeast by modulating interactions between the Mig1 repressor and the Cyc8-Tup1 co-repressor. EMBO Rep. 2004;5(4):368-372.
16. Hirota K, Hoffman CS, Ohta K. Reciprocal nuclear shuttling of two antagonizing Zn finger proteins modulates Tup family corepressor function to repress chromatin remodeling. Eukaryot Cell. 2006;5(12):1980-1989.
17. Vassiliadis D, Wong KH, Andrianopoulos A, et al. A genome-wide analysis of carbon catabolite repression in *Schizosaccharomyces pombe*. BMC Genomics. 2019;20(1):251.
18. Higuchi T, Watanabe Y, Yamamoto M. Protein kinase A regulates sexual development and gluconeogenesis through phosphorylation of the Zn finger transcriptional activator Rst2p in fission yeast. Mol Cell Biol. 2002;22(1):1-11.
19. Neely LA, Hoffman CS. Protein kinase A and mitogen-activated protein kinase pathways antagonistically regulate fission yeast *fbp1* transcription by employing different modes of action at two upstream activation sites. Mol Cell Biol. 2000;20(17):6426-6434.
20. Hoffman CS. Glucose sensing via the protein kinase A pathway in *Schizosaccharomyces pombe*. Biochem Soc Trans. 2005;33(1):257-260.

21. Shiozaki K, Russell P. Conjugation, meiosis, and the osmotic stress response are regulated by Spc1 kinase through Atf1 transcription factor in fission yeast. Genes Dev. 1996;10(18):2276-2288.

22. Madrid M, Soto T, Franco A, et al. A cooperative role for Atf1 and Pap1 in the detoxification of the oxidative stress induced by glucose deprivation in *Schizosaccharomyces pombe*. J Biol Chem. 2004;279(40):41594-41602.

23. Zuin A, Carmona M, Morales-Ivorra I, et al. Lifespan extension by calorie restriction relies on the Sty1 MAP kinase stress pathway. Embo J. 2010;29(5):981-991.

24. Asada R, Takemata N, Hoffman CS, et al. Antagonistic controls of chromatin and mRNA start site selection by Tup family corepressors and the CCAAT-binding factor. Mol Cell Biol. 2015; 35(5):847-855.

25. Oda A, Takemata N, Hirata Y, et al. Dynamic transition of transcription and chromatin landscape during fission yeast adaptation to glucose starvation. Genes Cells. 2015;20(5):392-407.

26. Galdieri L, Mehrotra S, Yu S, et al. Transcriptional regulation in yeast during diauxic shift and stationary phase. OMICS. 2010;14(6):629-638.

27. de Jong-Gubbels P, van Dijken JP, Pronk JT. Metabolic fluxes in chemostat cultures of *Schizosaccharomyces pombe* grown on mixtures of glucose and ethanol. Microbiology. 1996;142(6):1399-1407.

28. Tsai CS, Aveledo AJ, McDonald IJ, et al. Diauxic growth of the fission yeast *Schizosaccharomyces pombe* in mixtures of D-glucose and ethanol or acetate. Can J Microbiol. 1987;33(7):593-597.

29. Matsuzawa T, Ohashi T, Hosomi A, et al. The *gld1*$^{+}$ gene encoding glycerol dehydrogenase is required for glycerol metabolism in *Schizosaccharomyces pombe*. Appl Microbiol Biotechnol. 2010;87(2):715-727.

30. Rabinowitz JD, White E. Autophagy and metabolism. Science. 2010;330(6009):1344-1348.
31. Suzuki K, Kubota Y, Sekito T, et al. Hierarchy of Atg proteins in pre-autophagosomal structure organization. Genes Cells. 2007;12(2):209-218.
32. Noda NN, Fujioka Y. Atg1 family kinases in autophagy initiation. Cell Mol Life Sci. 2015;72(16):3083-3096.
33. Yeh YY, Wrasman K, Herman PK. Autophosphorylation within the Atg1 activation loop is required for both kinase activity and the induction of autophagy in *Saccharomyces cerevisiae*. Genetics. 2010;185(3):871-882.
34. Yeh YY, Shah KH, Herman PK. An Atg13 protein-mediated self-association of the Atg1 protein kinase is important for the induction of autophagy. J Biol Chem. 2011;286(33):28931-28939.
35. Hughes Hallett JE, Luo X, Capaldi AP. Snf1/AMPK promotes the formation of Kog1/Raptor-bodies to increase the activation threshold of TORC1 in budding yeast. eLife. 2015;4:e091181.
36. Kamada Y, Funakoshi T, Shintani T, et al. Tor-mediated induction of autophagy via an Apg1 protein kinase complex. J Cell Biol. 2000;150(6):1507-1513.
37. Kamada Y, Yoshino K, Kondo C, et al. Tor directly controls the Atg1 kinase complex to regulate autophagy. Mol Cell Biol. 2010;30(4):1049-1058.
38. Hu Z, Raucci S, Jaquenoud M, et al. Multilayered control of protein turnover by TORC1 and Atg1. Cell Rep. 2019;28(13):3486-3496.
39. Kim J, Kundu M, Viollet B, et al. AMPK and mTOR regulate autophagy through direct phosphorylation of Ulk1. Nat Cell Biol. 2011;13(2):132-141.

40. Yorimitsu T, Zaman S, Broach JR, et al. Protein kinase A and Sch9 cooperatively regulate induction of autophagy in *Saccharomyces cerevisiae*. Mol Biol Cell. 2007;18(10):4180-4189.

41. Graef M, Nunnari J. Mitochondria regulate autophagy by conserved signalling pathways. Embo J. 2011;30(11):2101-2114.

42. Yi C, Tong J, Lu P, et al. Formation of a Snf1-Mec1-Atg1 module on mitochondria governs energy deprivation-induced autophagy by regulating mitochondrial respiration. Dev Cell. 2017;41(1):59-71.

43. May AI, Prescott M, Ohsumi Y. Autophagy facilitates adaptation of budding yeast to respiratory growth by recycling serine for one-carbon metabolism. Nat Commun. 2020;11(1):5052.

44. Adachi A, Koizumi M, Ohsumi Y. Autophagy induction under carbon starvation conditions is negatively regulated by carbon catabolite repression. J Biol Chem. 2017;292(48):19905-19918.

45. Lang MJ, Martinez-Marquez JY, Prosser DC, et al. Glucose starvation inhibits autophagy via vacuolar hydrolysis and induces plasma membrane internalization by down-regulating recycling. J Biol Chem. 2014;289(24):16736-16747.

46. Pan ZQ, Shao GC, Liu XM, et al. Atg1 kinase in fission yeast is activated by Atg11-mediated dimerization and cis-autophosphorylation. eLife. 2020;9:e58073.

47. Corral-Ramos C, Barrios R, Ayté J, et al. TOR and MAP kinase pathways synergistically regulate autophagy in response to nutrient depletion in fission yeast. Autophagy. 2022;18(2):375-390.

48. Mukaiyama H, Kajiwara S, Hosomi A, et al. Autophagy-deficient *Schizosaccharomyces pombe* mutants undergo partial sporulation during nitrogen starvation. Microbiology. 2009;155(12):3816-3826.

936 49. Kohda TA, Tanaka K, Konomi M, et al. Fission yeast autophagy induced by nitrogen
937 starvation generates a nitrogen source that drives adaptation processes. Genes Cells.
938 2007;12(2):155-170.
939 50. Sun LL, Li M, Suo F, et al. Global analysis of fission yeast mating genes reveals new
940 autophagy factors. PLoS Genet. 2013;9(8):e1003715.
941 51. Matsuzawa T, Hara F, Tohda H, et al. Promotion of glycerol utilization using ethanol
942 and 1-propanol in *Schizosaccharomyces pombe*. Appl Microbiol Biotechnol.
943 2012;95(2):441-449.
944 52. Gross AS, Graef M. Mechanisms of autophagy in metabolic stress response. J Mol Biol.
945 2020;432(1):28-52.
946 53. Pan ZQ, Du LL. Atg11-mediated activation of Atg1 kinase in fission yeast. Autophagy.
947 2021;17(2):584-585.
948 54. Takeda K, Starzynski C, Mori A, et al. The critical glucose concentration for respiration-
949 independent proliferation of fission yeast, *Schizosaccharomyces pombe*.
950 Mitochondrion. 2015;22:91-95.
951 55. Jiang G, Liu Q, Kato T, et al. Role of mitochondrial complex III/IV in the activation of
952 transcription factor Rst2 in *Schizosaccharomyces pombe*. Mol Microbiol.
953 2021;115(6):1323-1338.
954 56. Zuin A, Gabrielli N, Calvo IA, et al. Mitochondrial dysfunction increases oxidative
955 stress and decreases chronological life span in fission yeast. PLoS One.
956 2008;3(7):e2842.
957 57. Yao W, Li Y, Wu L, et al. Atg11 is required for initiation of glucose starvation-induced
958 autophagy. Autophagy. 2020;16(12):2206-2218.

58. Lopez-Girona A, Tanaka K, Chen XB, et al. Serine-345 is required for Rad3-dependent phosphorylation and function of checkpoint kinase Chk1 in fission yeast. Proc Natl Acad Sci U S A. 2001;98(20):11289-11294.

59. Niederberger C, Schweingruber M. A *Schizosaccharomyces pombe* gene, *ksg1*, that shows structural homology to the human phosphoinositide-dependent protein kinase PDK1, is essential for growth, mating and sporulation. Mol Gen Genet. 1999;261(1):177-183.

60. Gupta DR, Paul SK, Oowatari Y, et al. Multistep regulation of protein kinase A in its localization, phosphorylation and binding with a regulatory subunit in fission yeast. Curr Genet. 2011;57(5):353-365.

61. Masuda F, Ishii M, Mori A, et al. Glucose restriction induces transient G2 cell cycle arrest extending cellular chronological lifespan. Sci Rep. 2016;6:19629.

62. Roux AE, Quissac A, Chartrand P, et al. Regulation of chronological aging in *Schizosaccharomyces pombe* by the protein kinases Pka1 and Sck2. Aging Cell. 2006;5(4):345-357.

63. Zuin A, Castellano-Esteve D, Ayte J, et al. Living on the edge: stress and activation of stress responses promote lifespan extension. Aging. 2010;2(4):231-237.

64. Alvers AL, Wood MS, Hu D, et al. Autophagy is required for extension of yeast chronological life span by rapamycin. Autophagy. 2009;5(6):847-849.

65. Perez P, Cansado J. Cell integrity signaling and response to stress in fission yeast. Current Protein & Peptide Science. 2010;11(8):680-692.

66. Chen D, Toone WM, Mata J, et al. Global transcriptional responses of fission yeast to environmental stress. Mol Biol Cell. 2003;14(1):214-229.

982 67. Lawrence CL, Maekawa H, Worthington JL, et al. Regulation of *Schizosaccharomyces*
983 *pombe* Atf1 protein levels by Sty1-mediated phosphorylation and heterodimerization
984 with Pcr1. J Biol Chem. 2007;282:5160-5170.
985 68. Dal Santo P, Blanchard B, Hoffman CS. The *Schizosaccharomyces pombe* Pyp1 protein
986 tyrosine phosphatase negatively regulates nutrient monitoring pathways. J Cell Sci.
987 1996;109 (7):1919-1925.
988 69. Davidson MK, Shandilya HK, Hirota K, et al. Atf1-Pcr1-M26 complex links stress-
989 activated MAPK and cAMP-dependent protein kinase pathways via chromatin
990 remodeling of *cgs2*$^{+}$. J Biol Chem. 2004;279 (49):50857-50863.
991 70. Liu J, Jia Y, Li J, et al. Transcriptional profiling analysis of individual kinase-deletion
992 strains of fission yeast in response to nitrogen starvation. Mol Genet Genomics.
993 2015;290(3):1067-1083.
994 71. Kunitomo H, Higuchi T, Iino Y, et al. A zinc-finger protein, Rst2p, regulates
995 transcription of the fission yeast *ste11*$^{+}$ gene, which encodes a pivotal transcription
996 factor for sexual development. Mol Biol Cell. 2000;11(9):3205-3217.
997 72. Hirota K, Hoffman CS, Shibata T, et al. Fission yeast Tup1-like repressors repress
998 chromatin remodeling at the *fbp1*$^{+}$ promoter and the ade6-M26 recombination hotspot.
999 Genetics. 2003;165(2):505-515.
1000 73. Mata J, Bähler J. Global roles of Ste11p, cell type, and pheromone in the control of gene
1001 expression during early sexual differentiation in fission yeast. Proc Natl Acad Sci U S
1002 A. 2006;103(42):15517-15522.
1003 74. Flores CL, Rodríguez C, Petit T, et al. Carbohydrate and energy-yielding metabolism
1004 in non-conventional yeasts. FEMS Microbiol Rev. 2000;24(4):507-529.

75. Tay YD, Leda M, Spanos C, et al. Fission Yeast NDR/LATS Kinase Orb6 regulates exocytosis via phosphorylation of the exocyst complex. Cell Rep. 2019;26(6):1654-1667.

76. Kettenbach AN, Deng L, Wu Y, et al. Quantitative phosphoproteomics reveals pathways for coordination of cell growth and division by the conserved fission yeast kinase pom1. Mol Cell Proteomics. 2015;14(5):1275-1287.

77. Swaffer MP, Jones AW, Flynn HR, et al. CDK Substrate phosphorylation and ordering the cell cycle. Cell. 2016;167(7):1750-1761.

78. Davie E, Forte GM, Petersen J. Nitrogen regulates AMPK to control TORC1 signaling. Curr Biol. 2015;25(4):445-54.

79. Miller-Fleming L, Antas P, Pais TF, et al. Yeast DJ-1 superfamily members are required for diauxic-shift reprogramming and cell survival in stationary phase. Proc Natl Acad Sci U S A. 2014;111(19):7012-7017.

80. Stephan JS, Yeh YY, Ramachandran V, et al. The Tor and PKA signaling pathways independently target the Atg1/Atg13 protein kinase complex to control autophagy. Proc Natl Acad Sci U S A. 2009;106(40):17049-17054.

81. Budovskaya YV, Stephan JS, Reggiori F, et al. The Ras/cAMP-dependent protein kinase signaling pathway regulates an early step of the autophagy process in *Saccharomyces cerevisiae*. J Biol Chem. 2004;279(20):20663-20671.

82. Budovskaya YV, Stephan JS, Deminoff SJ, et al. An evolutionary proteomics approach identifies substrates of the cAMP-dependent protein kinase. Proc Natl Acad Sci U S A. 2005;102(39):13933-13938.

83. Schmelzle T, Beck T, Martin DE, et al. Activation of the RAS/cyclic AMP pathway suppresses a TOR deficiency in yeast. Mol Cell Biol. 2004;24(1):338-351.

84. Sanso M, Gogol M, Ayte J, et al. Transcription factors Pcr1 and Atf1 have distinct roles in stress- and Sty1-dependent gene regulation. Eukaryot Cell. 2008;7(5):826-835.

85. Lopez-Aviles S, Grande M, Gonzalez M, et al. Inactivation of the Cdc25 phosphatase by the stress-activated Srk1 kinase in fission yeast. Mol Cell. 2005;17(1):49-59.

86. Prieto-Ruiz F, Vicente-Soler J, Franco A, et al. RNA-Binding Protein Rnc1 regulates cell length at division and acute stress response in fission yeast through negative feedback modulation of the Stress-Activated Mitogen-Activated Protein Kinase pathway. mBio. 2020;11(1):e02815-19.

87. Malecki M, Bitton DA, Rodríguez-López M, et al. Functional and regulatory profiling of energy metabolism in fission yeast. Genome Biol. 2016;17(1):240.

88. Kim DU, Hayles J, Kim D, et al. Analysis of a genome-wide set of gene deletions in the fission yeast *Schizosaccharomyces pombe*. Nat Biotechnol. 2010;28(6):617-623.

89. Hentges P, Van Driessche B, Tafforeau L, et al. Three novel antibiotic marker cassettes for gene disruption and marker switching in *Schizosaccharomyces pombe.* Yeast. 2005;22(13):1013-1019.

90. Sato M, Dhut S, Toda T. New drug-resistant cassettes for gene disruption and epitope tagging in *Schizosaccharomyces pombe*. Yeast. 2005;22(7):583-591.

91. Petersen J, Russell P. Growth and the environment of *Schizosaccharomyces pombe*. Cold Spring Harb Protoc. 2016;2016(3):pdb.top079764.

92. Moreno S, Klar A, Nurse P. Molecular genetic analysis of fission yeast *Schizosaccharomyces pombe*. Methods Enzymol.1991;194:795-823.

93. Mi H, Muruganujan A, Thomas PD. PANTHER in 2013: modeling the evolution of gene function, and other gene attributes, in the context of phylogenetic trees. Nucleic Acids Res. 2013;41:D377-86.

94. Lock A, Rutherford K, Harris MA, et al. PomBase 2018: user-driven reimplementation of the fission yeast database provides rapid and intuitive access to diverse, interconnected information. Nucleic Acids Res. 2019;47(D1):D821-d827.

95. Grallert A, Hagan IM. Preparation of protein extracts from *Schizosaccharomyces pombe* using trichloroacetic acid precipitation. Cold Spring Harb Protoc. 2017;2017(2).

96. Schneider C, Rasband W, Eliceiri K. NIH Image to ImageJ: 25 years of image analysis. Nat Methods. 2012;9(7):671-675.

Figure legends

Figure 1. Induction of autophagy in response to limited glucose availability. (**A**) Exponentially growing *S. pombe* wild-type cells expressing a CFP-Atg8 fusion were grown in EMM2 with 7% glucose (Glu), were recovered by filtration, and resuspended for the indicated times in the same medium with increased amounts of Glu (0 to 0.2%) in the presence of 3% glycerol (Gly). The percentage of cells with visible CFP-Atg8 puncta was estimated at each time point by fluorescence microscopy (number of cells $\geq$300; three biological replicates), and is represented as mean $\pm$ SD. (**B**) Representative micrographs of cell samples from (A) after 3 h of incubation were observed by fluorescence microscopy. Arrows: CFP-Atg8 puncta. (**C**) Cell samples from the indicated time points were extracted with TCA, and subjected to western blot analysis with anti-GFP antibody (CFP-Atg8 fusion and proteolysis), and normalized with anti-Cdc2 (internal loading control). CFP-Atg8 proteolysis was quantified by determining the signal ratio of the CFP-Atg8 band with respect to the free CFP band. Data are shown as mean $\pm$ SD, and correspond to biological triplicates. (**D**) The percentage of cells with visible CFP-Atg8 puncta in *S. pombe* strains of the indicated genotypes expressing a CFP-Atg8 fusion was estimated at each time point by fluorescence microscopy as described in (A). (**E**) Representative fluorescence microscopy images of cell samples from (D) were taken after 4 h of incubation. (**F**) Cell samples corresponding to the indicated time points were extracted with TCA, and subjected to western blot analysis with anti-GFP antibody (CFP-Atg8 fusion and proteolysis), and normalized with anti-Cdc2 (internal loading control). Results from a representative experiment are shown. (**G**) *S. pombe* wild-type cells expressing a Atg1-HA genomic fusion were grown in EMM2 with 7% Glu and resuspended in the same medium with 3% Gly plus 0.04% Glu or 3% Gly for the indicated times. Total Atg1 was detected by immunoblotting of TCA-precipitated protein extracts with anti-HA antibody. *, lower mobility bands. Anti-Cdc2 was used as a loading control. Results from a representative experiment are shown.

Figure 2. Mitochondrial respiration is critical for glucose-dependent induction of autophagy. (**A**) Basic architecture of the electron transport chain (ETC). Specific complex components and inhibitors employed in this work are shown. (**B**) Exponentially growing *S. pombe* wild-type cells expressing a CFP-Atg8 fusion were grown in EMM2 with 7% glucose (Glu) and incubated in the same medium with 0.04% Glu plus 3% glycerol (Gly) with or without (dimethyl sulfoxide: DMSO; solvent control), 0.5 μM AA for the indicated times. The percentage of cells with visible CFP-Atg8 puncta was estimated at each time point by fluorescence microscopy (number of cells ≥300; three biological replicates), and is represented as mean ± SD. Representative fluorescence microscopy images of cell samples from were taken at 0 and 4 h of incubation are shown below. Arrows: CFP-Atg8 puncta. (**C**) Exponentially growing *S. pombe* wild-type cells expressing a CFP-Atg8 fusion were incubated with 0.04% Glu plus 3% Gly with or without 0.5 μM AA for the indicated times. Cell samples were extracted with TCA and subjected to western blot analysis with anti-GFP antibody (CFP-Atg8 fusion and proteolysis), and normalized with anti-Cdc2 (internal loading control). Data for CFP-Atg8 proteolysis are shown as mean ± SD, and correspond to biological triplicates. (**D**) *S. pombe* wild-type cells expressing a Atg1-HA genomic fusion were grown in EMM2 with 7% Glu and resuspended in the same medium with 0.04% Glu plus 3% Gly with or without 0.5 μM AA for the indicated times. Total Atg1 was detected by immunoblotting of TCA-precipitated protein extracts with anti-HA antibody. *, lower mobility bands. Anti-Cdc2 was used as a loading control. Results from a representative experiment are shown. (**E**) CFP-Atg8 proteolysis of exponentially growing *S. pombe* wild-type cells expressing a CFP-Atg8 fusion incubated in medium with 0.04% Glu plus 3% Gly without further treatment (untreated), or treated with either 25.6 μg/ml rotenone, 2 mM TTFA, 10 μM oligomycin, or 500 μM DCCD. Data for CFP-Atg8 proteolysis are shown as mean ± SD, and correspond to biological triplicates. ns, not

significant, ****, $p < 0.0001$, **, $p < 0.01$, as calculated by one-way ANOVA. (**F**) CFP-Atg8 proteolysis of exponentially growing *S. pombe* wild-type cells and ETC mutants *nde1*Δ*, rip1*Δ*, qcr2*Δ, and *atp11*Δ expressing a CFP-Atg8 fusion incubated in medium with 0.04% Glu plus 3% Gly. Data for CFP-Atg8 proteolysis are shown as mean ± SD, and correspond to biological triplicates. ns, not significant, ****, $p < 0.0001$, as calculated by one-way ANOVA. (**G**) Oxygen consumption of the indicated strains grown in EMM2 7% Glu was determined from logarithmic cultures at low OD_{600} (10-30% of the maximum OD_{600}). Data are shown as mean ± SD, and correspond to biological triplicates. ****, $p < 0.0001$; *, $p < 0.05$, as calculated by one-way ANOVA. (**H**) CFP-Atg8 proteolysis of exponentially growing *S. pombe* wild-type cells and mutants of the indicated genotypes expressing a CFP-Atg8 fusion and incubated in medium with 0.04% Glu plus 3% Gly. Data are shown as mean ± SD, and correspond to biological triplicates. ns, not significant, as calculated by one-way ANOVA. (**I**) Decimal dilutions of strains of the indicated genotypes were spotted on YES solid plates with 2% Glu or 0.04% Glu plus 3% Gly. The plates were incubated at 30ºC for 3 days, and photographed. A representative experiment is shown.

Figure 3. cAMP-protein kinase A signaling represses *S. pombe* autophagy in response to glucose limitation or starvation. (**A**) The cAMP-protein kinase A signaling pathway in *S. pombe*. Please see text for a detailed description of its main components and functions. (**B**) Exponentially growing *S. pombe* strains of the indicated genotypes expressing a CFP-Atg8 fusion were grown in EMM2 with 7% glucose (Glu), recovered by filtration, and resuspended for the indicated times in the same medium lacking Glu with 3% glycerol (Gly). The percentage of cells with visible CFP-Atg8 puncta was estimated at each time point by fluorescence microscopy (number of cells ≥300; three biological replicates), and is represented as mean ± SD. (**C**) Representative micrographs of cell samples from (B) after 0.5 h of incubation were

observed by fluorescence microscopy. (**D**) Cell samples from the indicated time points were extracted with TCA, subjected to western blot analysis with anti-GFP antibody (CFP-Atg8 fusion and proteolysis), and normalized with anti-Cdc2 (internal loading control). Data for CFP-Atg8 proteolysis are shown as mean ± SD, and correspond to biological triplicates. (**E**) Exponentially growing *S. pombe* wild-type and *pka1*Δ cells expressing an Atg1-HA genomic fusion were grown in EMM2 with 7% Glu and resuspended in the same medium lacking Glu plus 3% Gly for the indicated times. Total Atg1 was detected by immunoblotting of TCA-precipitated protein extracts with anti-HA antibody. *, lower mobility bands. Anti-Cdc2 was used as a loading control. Results from a representative experiment are shown. (**F**) CFP-Atg8 proteolysis was quantified at each time point for the indicated strains as described in (D). ****, $p < 0.0001$; *, $p < 0.05$, as calculated by one-way ANOVA. (**G**) CFP-Atg8 fusion and proteolysis to the indicated strains were followed at the indicated times by western blot analysis. Results from a representative experiment are shown. (**H**) CFP-Atg8 proteolysis was quantified at each time point for the indicated strains growing in 3% Gly with or without 0.5 µM AA. Results from a representative experiment are shown. (**I**) CFP-Atg8 proteolysis was quantified at each time point for the indicated strains as described in (D). ns, not significant, as calculated by one-way ANOVA. (**J**) *S. pombe* wild-type, *pka1*Δ, *atg1*Δ, and *atg1*Δ *pka1*Δ cells were grown in EMM2 with 7% Glu, recovered by filtration and incubated in medium lacking Glu for 7 days, or pre-incubated low Glu medium (0.08%) for 6 h, and then incubated for 7 days without Glu. Cell viability in each sample was measured by counting the colony-forming units (CFU; 3 days at 30ºC), and is expressed as the ratio of the number of colonies formed *vs.* the total number of cells plated. The averages of three independent experiments ± SD are shown. ****, $p < 0.0001$; *, $p < 0.05$; ns, not significant, as calculated by one-way ANOVA.

Figure 4. The cAMP-PKA and SAPK pathways partially regulate autophagy upon glucose limitation or starvation through the transcription factors Rst2 and Atf1, respectively. (**A**) Exponentially growing *S. pombe* wild-type and *rst2*Δ cells expressing a CFP-Atg8 fusion were grown in EMM2 with 7% glucose (Glu), and incubated in the same medium with 0.04% Glu plus 3% glycerol (Gly) for the indicated times. The percentage of cells with visible CFP-Atg8 puncta was estimated at each time point by fluorescence microscopy (number of cells $\geq$300; three biological replicates), and is represented as mean $\pm$ SD. **, $p<0.01$; ns, not significant, as calculated by one-way ANOVA. (**B**) Exponentially growing *S. pombe* wild-type and *rst2*Δ cells expressing a CFP-Atg8 fusion were grown in EMM2 with 7% Glu and resuspended in the same medium with 0.04% Glu plus 3% Gly. CFP-Atg8 fusion and proteolysis were monitored at the indicated times by western blot analysis with anti-GFP antibody and normalized with anti-Cdc2 (internal loading control). Data for CFP-Atg8 proteolysis are shown as mean $\pm$ SD, and correspond to biological triplicates. **, $p<0.01$; *, $p<0.05$, as calculated by one-way ANOVA. (**C**) The percentage of cells with visible CFP-Atg8 puncta was estimated for the indicated strains and time points as described in (A). Representative fluorescence microscopy images of cell samples taken after 0.5 h of incubation are shown below. (**D**) CFP-Atg8 proteolysis was quantified for the indicated strains at each time point as described in (B). Data are shown as mean $\pm$ SD, and correspond to biological triplicates. (**E**) CFP-Atg8 fusion and proteolysis were followed in the indicated strains incubated in EMM2 lacking Glu with 3% Gly. Results from a representative experiment are shown. (**F**) CFP-Atg8 fusion and proteolysis were followed in the indicated strains incubated in EMM2 medium with 7% Glu and resuspended in the same medium with 0.04% Glu plus 3% Gly. Results from a representative experiment are shown. (**G**) CFP-Atg8 proteolysis was quantified for the indicated strains at each time point as described in (B). Data are shown as mean $\pm$ SD, and correspond to biological triplicates. **, $p<0.01$; *, $p<0.05$; ns, not significant, as calculated by one-way ANOVA. (**H**)

CFP-Atg8 proteolysis was quantified for the indicated strains at each time point as described in (B) Data are shown as mean ± SD, and correspond to biological triplicates.

Figure 5. Enhanced expression of glycerol assimilatory genes by Rst2 and Atf1 transcription factors is important for respiration-dependent induction of autophagy upon glucose limitation. (**A**) Venn diagrams indicating the overlap in the number of differentially expressed, upregulated genes in *pka1*Δ cells whose expression relies on Rst2, Atf1, or both transcription factors. (**B**) GO enrichment analysis (biological process) of relevant categories identified within the 145 upregulated genes found in *pka1*Δ cells whose expression depends upon both Rst2 and Atf1 transcription factors. (**C**) Comparative heatmap of Log_2FC in *pka1*Δ*, pka1*Δ *rst2*Δ*,* and *pka1*Δ *atf1*Δ mutants for the identified genes involved in glycerol metabolism (GO:0006071). A metabolic map of glycerol metabolism genes in *S. pombe* is also shown. Genes identified in the microarray experiments are marked in red. (**D**) mRNA levels of the indicated genes were measured by qPCR from total RNA extracted from cell samples corresponding to *S. pombe* wild-type, *pka1*Δ, *pka1*Δ *rst2*Δ, and *pka1*Δ *atf1*Δ cells growing exponentially in EMM2 with 7% glucose. Results are shown as relative fold expression (mean ± SD) from three biological repeats. ****, $p<0.0001$; ***, $p<0.001$; **, $p<0.01$, as calculated by one-way ANOVA. (**E**) The expression levels of a genomic Gld1-HA fusion were determined in growing cells from the indicated genotypes growing exponentially in EMM2 with 7% glucose, and resuspended in the same medium with 0.04% glucose plus 3% glycerol (upper panel) or 3% glycerol alone (lower panel). Results are shown as relative fold expression (mean ± SD) from three biological repeats. ****, $p<0.0001$; ns, not significant, as calculated by one-way ANOVA. (**F**) mRNA levels of the indicated genes were measured by qPCR from total RNA extracted from cell samples corresponding to *S. pombe* wild-type, *rst2*Δ, and *atf1Δ* cells after 0 and 2 h of incubation in EMM2 with 0.04% glucose (Glu) plus 3% glycerol (Gly). Results are shown as relative fold

expression (mean ± SD) from three biological repeats. ****, $p<0.0001$; ns, not significant, as calculated by one-way ANOVA. (**G**) Exponentially growing *S. pombe* wild-type and mutant strains expressing a CFP-Atg8 fusion were grown in EMM2 medium with 7% Glu and resuspended in the same medium with 0.04% Glu plus 3% Gly. CFP-Atg8 fusion and proteolysis were monitored at the indicated times by western blot analysis with anti-GFP antibody and normalized with anti-Cdc2 (internal loading control). Data for CFP-Atg8 proteolysis are shown as mean ± SD, and correspond to biological triplicates. ****, $p<0.0001$; ns, not significant, as calculated by one-way ANOVA. (**H**) CFP-Atg8 proteolysis was quantified for the indicated strains incubated in medium with 3% Gly at each time point as described in (G). Data are shown as mean ± SD, and correspond to biological triplicates. ****, $p<0.0001$, as calculated by one-way ANOVA.

Figure 6. *In vivo* phosphorylation of Rst2 at S292 by Sty1 positively modulates its transcriptional activity during induction of autophagy. (**A**) The indicated wild-type and mutant strains expressing a Rst2-3HA genomic fusion were grown in EMM2 with 7% glucose (Glu), and resuspended in the same medium with 0.04% Glu plus 3% glycerol (Gly) for the indicated times. Total Rst2 levels were determined by immunoblotting of TCA-precipitated protein extracts with anti-HA antibody. Anti-Cdc2 was used as a loading control. Results from a representative experiment are shown. "*" shows the lower mobility and hyperphosphorylated protein band. (**B**) The indicated wild-type and mutant strains expressing a Rst2-3HA genomic fusion were grown in EMM2 with 7% Glu, resuspended in medium lacking Glu plus 3% Gly for the indicated times, and total Rst2 levels were determined as described in (A). (**C**) Basic structure of Rst2. Known Pka1-dependent phosphorylation sites appear colored in light blue. Putative S/T MAPK-phospho sites are colored in red. C2H2: zinc finger-type domain. (**D**) Wildtype, *rst2Δ*, and *sty1Δ* strains were grown in EMM2 with 7% Glu, and resuspended in the

same medium with 0.04% Glu plus 3% Gly for the indicated times. Rst2 phosphorylation at S292 was detected by immunoblotting of urea-denatured protein extracts with anti-phospho-S292 antibody. Anti-Cdc2 was used as a loading control. Results from a representative experiment are shown. (**E**) mRNA levels of the indicated genes were measured by qPCR from total RNA extracted from cell samples corresponding to *S. pombe* wild-type and mutant strains growing exponentially in EMM2 with 7% Glu. Results are shown as relative fold expression (mean ± SD) from three biological repeats. ****, $p<0.0001$; **, $p<0.01$; *, $p<0.05$; ns, not significant, as calculated by one-way ANOVA. (**F**) Upper panel: Exponentially growing *S. pombe* Rst2-HA (WT) and Rst2-S292A-HA cells expressing a CFP-Atg8 fusion were grown in EMM2 with 7% Glu, and incubated in the same medium with 0.04% Glu plus 3% Gly for the indicated times. The percentage of cells with visible CFP-Atg8 puncta was estimated at each time point by fluorescence microscopy (number of cells ≥300; three biological replicates), and is represented as mean ± SD. Lower panel: Data for CFP-Atg8 proteolysis at the indicated times are shown as mean ± SD, and correspond to biological triplicates. ****, $p<0.0001$; ***, $p<0.001$; **, $p<0.01$, as calculated by one-way ANOVA. (**G**) Upper panel: Exponentially growing *S. pombe pka1*Δ Rst2-HA and *pka1*Δ Rst2-S292A-HA cells expressing a CFP-Atg8 fusion were grown in EMM2 with 7% Glu, and incubated in the same medium lacking Glu with 3% Gly for the indicated times. The percentage of cells with visible CFP-Atg8 puncta was estimated at each time point by fluorescence microscopy (number of cells ≥300; three biological replicates), and is represented as mean ± SD. Lower panel: Data for CFP-Atg8 proteolysis at the indicated times are shown as mean ± SD, and correspond to biological triplicates. ****, $p<0.0001$; *, $p<0.05$, as calculated by one-way ANOVA.

Figure 7. Model depicting the signaling pathways and mechanisms that regulate the induction of autophagy in *S. pombe* during the transition from fermentative to respiratory metabolism. For specific details, please see text.

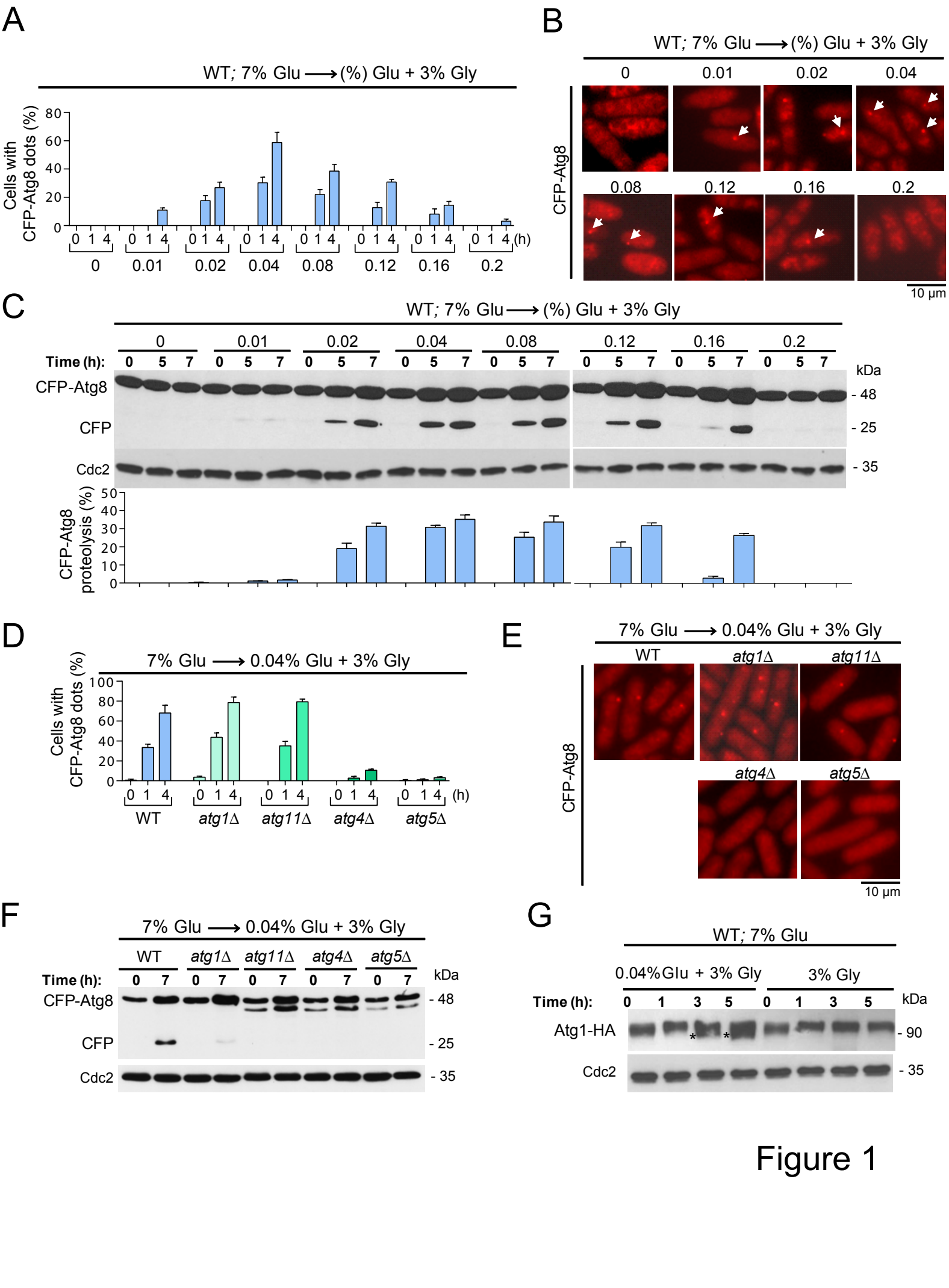
A
WT; 7% Glu ⟶ (%) Glu + 3% Gly
Cells with CFP-Atg8 dots (%)
0 1 4 (h)
0 0.01 0.02 0.04 0.08 0.12 0.16 0.2
B
WT; 7% Glu ⟶ (%) Glu + 3% Gly
CFP-Atg8
10 μm
C
WT; 7% Glu ⟶ (%) Glu + 3% Gly
Time (h):
CFP-Atg8
CFP
Cdc2
kDa
- 48
- 25
- 35
CFP-Atg8 proteolysis (%)
D
7% Glu ⟶ 0.04% Glu + 3% Gly
Cells with CFP-Atg8 dots (%)
WT atg1Δ atg11Δ atg4Δ atg5Δ
E
7% Glu ⟶ 0.04% Glu + 3% Gly
WT atg1Δ atg11Δ atg4Δ atg5Δ
CFP-Atg8
10 μm
F
7% Glu ⟶ 0.04% Glu + 3% Gly
WT atg1Δ atg11Δ atg4Δ atg5Δ
Time (h):
CFP-Atg8
CFP
Cdc2
kDa
- 48
- 25
- 35
G
WT; 7% Glu
0.04%Glu + 3% Gly
3% Gly
Time (h):
Atg1-HA
Cdc2
kDa
- 90
- 35

Figure 1

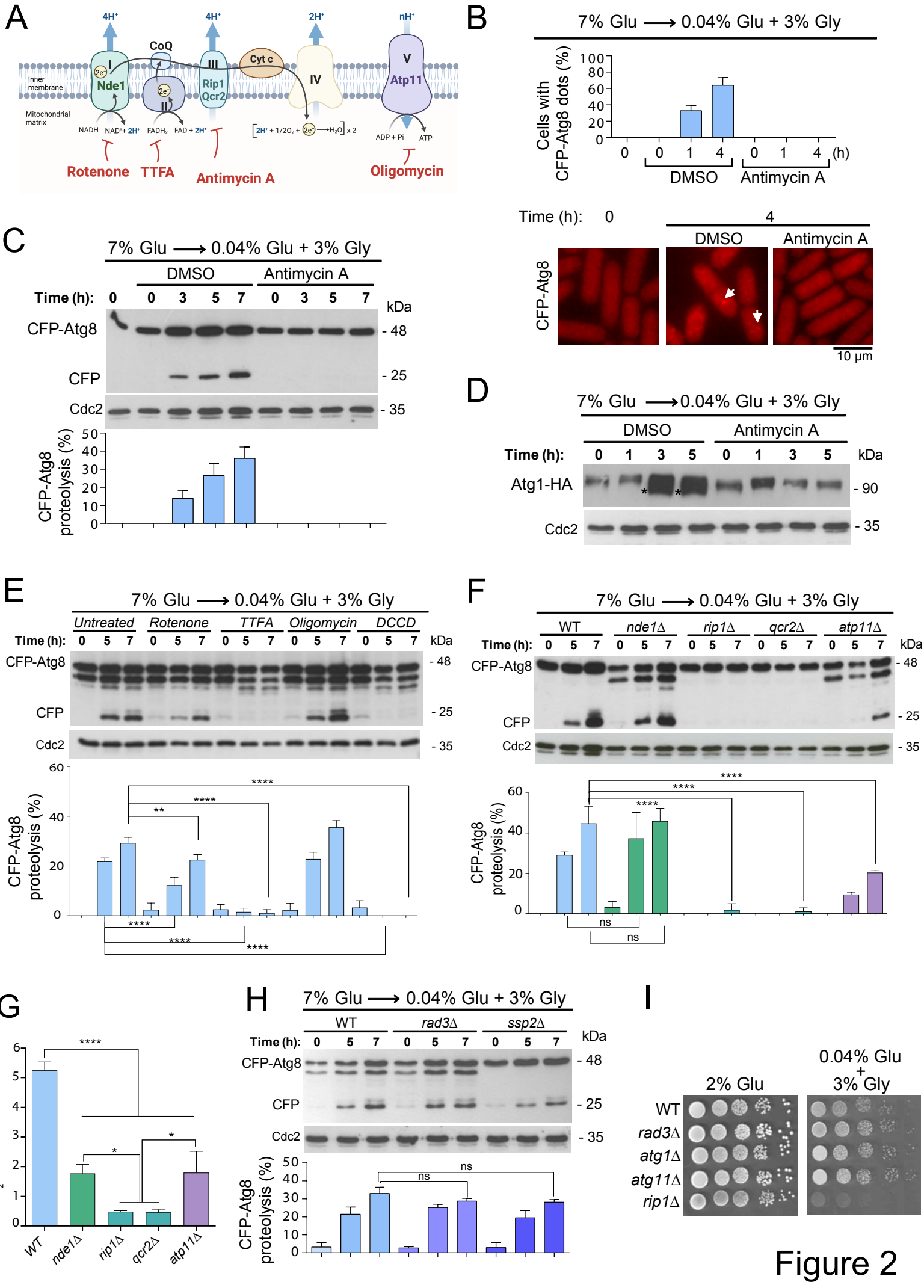
A
4H+
4H+
2H+
nH+
CoQ
Cyt c
Inner membrane
Mitochondrial matrix
Nde1
Rip1 Qcr2
Atp11
NADH
NAD+ + 2H+
FADH2
FAD + 2H+
ADP + Pi
ATP
Rotenone
TTFA
Antimycin A
Oligomycin
B
7% Glu ⟶ 0.04% Glu + 3% Gly
Cells with CFP-Atg8 dots (%)
DMSO
Antimycin A
(h)
Time (h): 0
4
DMSO
Antimycin A
CFP-Atg8
10 µm
C
7% Glu ⟶ 0.04% Glu + 3% Gly
DMSO
Antimycin A
Time (h):
kDa
CFP-Atg8
CFP
Cdc2
- 48
- 25
- 35
CFP-Atg8 proteolysis (%)
D
7% Glu ⟶0.04% Glu + 3% Gly
DMSO
Antimycin A
Time (h):
kDa
Atg1-HA
Cdc2
- 90
- 35
E
7% Glu ⟶ 0.04% Glu + 3% Gly
Untreated
Rotenone
TTFA
Oligomycin
DCCD
Time (h):
kDa
CFP-Atg8
CFP
Cdc2
- 48
- 25
- 35
CFP-Atg8 proteolysis (%)
F
7% Glu ⟶ 0.04% Glu + 3% Gly
WT
nde1Δ
rip1Δ
qcr2Δ
atp11Δ
Time (h):
kDa
CFP-Atg8
CFP
Cdc2
- 48
- 25
- 35
CFP-Atg8 proteolysis (%)
ns
G
% O2 consumed/2x10^7 cells
WT
nde1Δ
rip1Δ
qcr2Δ
atp11Δ
H
7% Glu ⟶ 0.04% Glu + 3% Gly
WT
rad3Δ
ssp2Δ
Time (h):
kDa
CFP-Atg8
CFP
Cdc2
- 48
- 25
- 35
CFP-Atg8 proteolysis (%)
ns
I
2% Glu
0.04% Glu + 3% Gly
WT
rad3Δ
atg1Δ
atg11Δ
rip1Δ

Figure 2

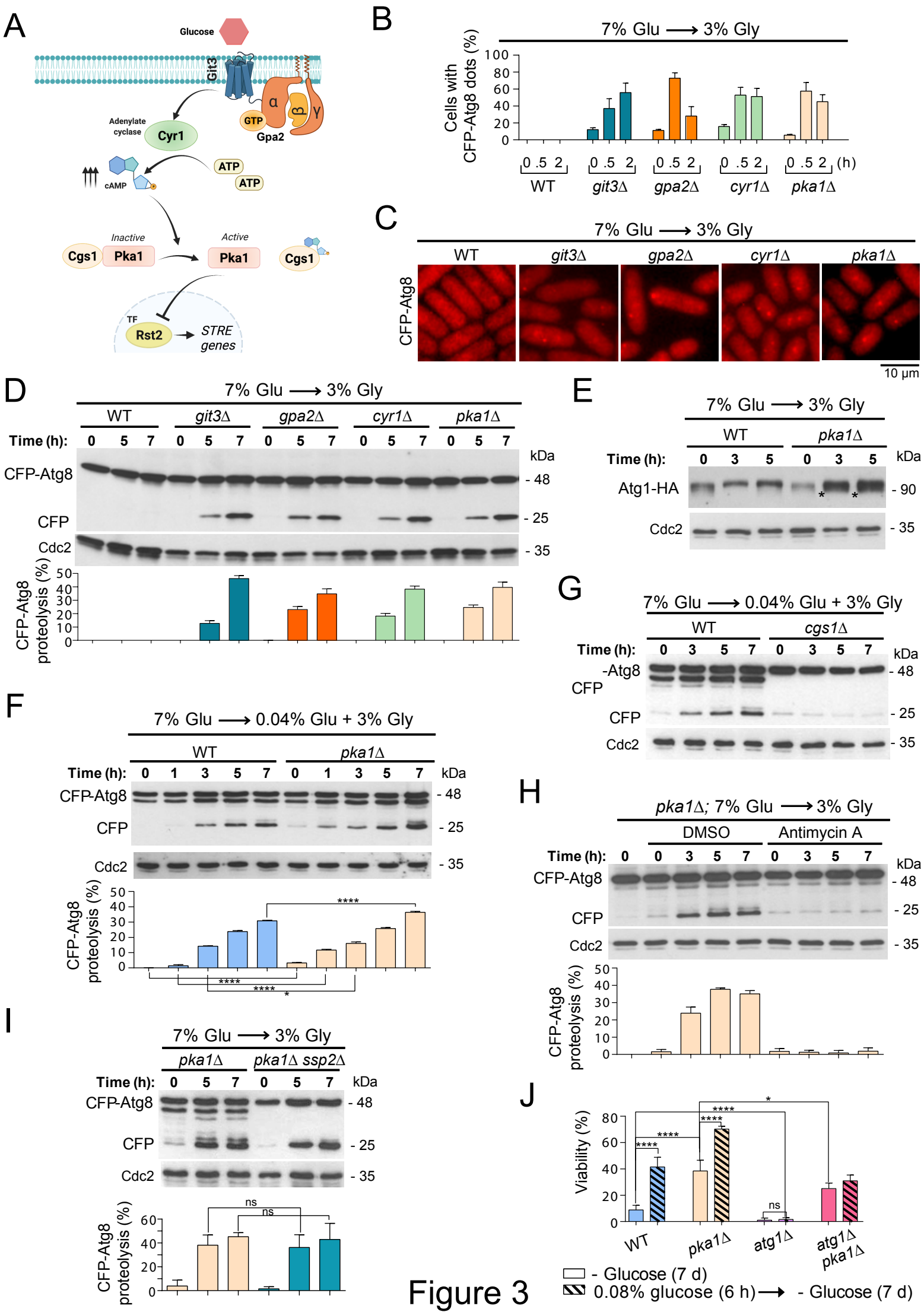
A
Glucose
Git3
α
β
γ
GTP
Gpa2
Adenylate cyclase
Cyr1
cAMP
ATP
ATP
Inactive
Active
Cgs1
Pka1
Pka1
Cgs1
TF
Rst2
STRE genes
B
7% Glu ⟶ 3% Gly
Cells with CFP-Atg8 dots (%)
100
80
60
40
20
0
0 .5 2
(h)
WT
git3Δ
gpa2Δ
cyr1Δ
pka1Δ
C
7% Glu ⟶ 3% Gly
WT
git3Δ
gpa2Δ
cyr1Δ
pka1Δ
CFP-Atg8
10 μm
D
7% Glu ⟶ 3% Gly
WT
git3Δ
gpa2Δ
cyr1Δ
pka1Δ
Time (h):
0 5 7 0 5 7 0 5 7 0 5 7 0 5 7
kDa
CFP-Atg8
- 48
CFP
- 25
Cdc2
- 35
CFP-Atg8 proteolysis (%)
50
40
30
20
10
0
E
7% Glu ⟶ 3% Gly
WT
pka1Δ
Time (h):
0 3 5 0 3 5
kDa
Atg1-HA
- 90
Cdc2
- 35
G
7% Glu ⟶ 0.04% Glu + 3% Gly
WT
cgs1Δ
Time (h):
0 3 5 7 0 3 5 7
kDa
-Atg8
CFP
- 48
CFP
- 25
Cdc2
- 35
F
7% Glu ⟶ 0.04% Glu + 3% Gly
WT
pka1Δ
Time (h):
0 1 3 5 7 0 1 3 5 7
kDa
CFP-Atg8
- 48
CFP
- 25
Cdc2
- 35
CFP-Atg8 proteolysis (%)
50
40
30
20
10
0
****
****
****
*
H
pka1Δ; 7% Glu ⟶ 3% Gly
DMSO
Antimycin A
Time (h):
0 0 3 5 7 0 3 5 7
kDa
CFP-Atg8
- 48
CFP
- 25
Cdc2
- 35
CFP-Atg8 proteolysis (%)
50
40
30
20
10
0
I
7% Glu ⟶ 3% Gly
pka1Δ
pka1Δ ssp2Δ
Time (h):
0 5 7 0 5 7
kDa
CFP-Atg8
- 48
CFP
- 25
Cdc2
- 35
CFP-Atg8 proteolysis (%)
60
40
20
0
ns
ns
J
Viability (%)
80
60
40
20
0
****
****
****
****
*
ns
WT
pka1Δ
atg1Δ
atg1Δ pka1Δ
- Glucose (7 d)
0.08% glucose (6 h) ⟶ - Glucose (7 d)

Figure 3

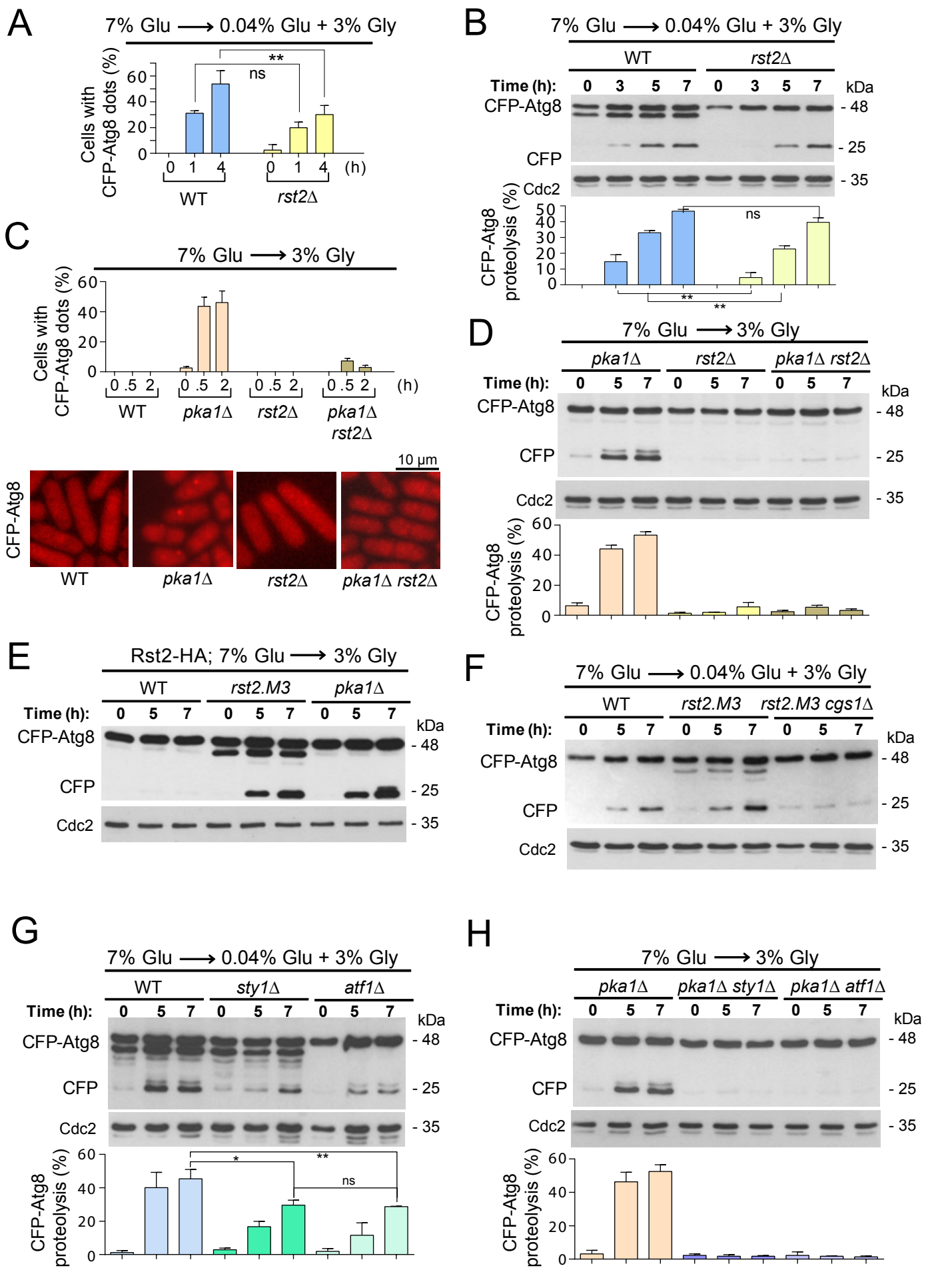
A
7% Glu ⟶ 0.04% Glu + 3% Gly
Cells with CFP-Atg8 dots (%)
**
ns
0 1 4 0 1 4 (h)
WT
rst2Δ
B
7% Glu ⟶ 0.04% Glu + 3% Gly
WT
rst2Δ
Time (h): 0 3 5 7 0 3 5 7
kDa
CFP-Atg8
CFP
Cdc2
- 48
- 25
- 35
CFP-Atg8 proteolysis (%)
ns
**
**
C
7% Glu ⟶ 3% Gly
Cells with CFP-Atg8 dots (%)
0 .5 2 0 .5 2 0 .5 2 0 .5 2 (h)
WT
pka1Δ
rst2Δ
pka1Δ rst2Δ
10 μm
CFP-Atg8
WT
pka1Δ
rst2Δ
pka1Δ rst2Δ
D
7% Glu ⟶ 3% Gly
pka1Δ
rst2Δ
pka1Δ rst2Δ
Time (h): 0 5 7 0 5 7 0 5 7
kDa
CFP-Atg8
CFP
Cdc2
- 48
- 25
- 35
CFP-Atg8 proteolysis (%)
E
Rst2-HA; 7% Glu ⟶ 3% Gly
WT
rst2.M3
pka1Δ
Time (h): 0 5 7 0 5 7 0 5 7
kDa
CFP-Atg8
CFP
Cdc2
- 48
- 25
- 35
F
7% Glu ⟶ 0.04% Glu + 3% Gly
WT
rst2.M3
rst2.M3 cgs1Δ
Time (h): 0 5 7 0 5 7 0 5 7
kDa
CFP-Atg8
CFP
Cdc2
- 48
- 25
- 35
G
7% Glu ⟶ 0.04% Glu + 3% Gly
WT
sty1Δ
atf1Δ
Time (h): 0 5 7 0 5 7 0 5 7
kDa
CFP-Atg8
CFP
Cdc2
- 48
- 25
- 35
CFP-Atg8 proteolysis (%)
*
**
ns
H
7% Glu ⟶ 3% Gly
pka1Δ
pka1Δ sty1Δ
pka1Δ atf1Δ
Time (h): 0 5 7 0 5 7 0 5 7
kDa
CFP-Atg8
CFP
Cdc2
- 48
- 25
- 35
CFP-Atg8 proteolysis (%)

Figure 4

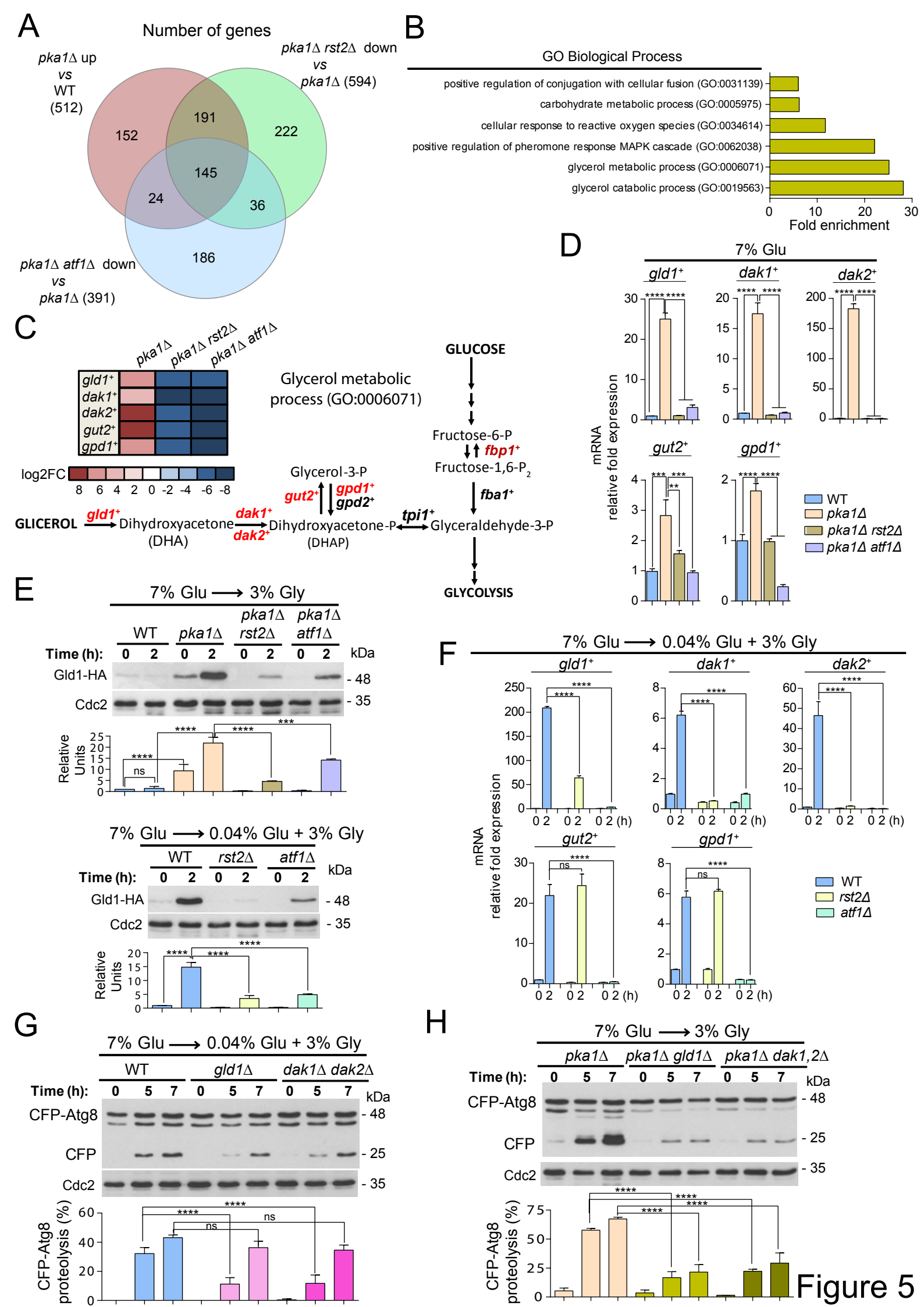
A
Number of genes
pka1Δ up vs WT (512)
pka1Δ rst2Δ down vs pka1Δ (594)
pka1Δ atf1Δ down vs pka1Δ (391)
152
191
222
145
24
36
186
B
GO Biological Process
positive regulation of conjugation with cellular fusion (GO:0031139)
carbohydrate metabolic process (GO:0005975)
cellular response to reactive oxygen species (GO:0034614)
positive regulation of pheromone response MAPK cascade (GO:0062038)
glycerol metabolic process (GO:0006071)
glycerol catabolic process (GO:0019563)
0 10 20 30
Fold enrichment
C
pka1Δ
pka1Δ rst2Δ
pka1Δ atf1Δ
gld1+
dak1+
dak2+
gut2+
gpd1+
log2FC
8 6 4 2 0 -2 -4 -6 -8
Glycerol metabolic process (GO:0006071)
GLUCOSE
Fructose-6-P
fbp1+
Fructose-1,6-P2
fba1+
Glycerol-3-P
gut2+
gpd1+ gpd2+
tpi1+
GLICEROL
gld1+
Dihydroxyacetone (DHA)
dak1+ dak2+
Dihydroxyacetone-P (DHAP)
Glyceraldehyde-3-P
GLYCOLYSIS
D
7% Glu
gld1+
dak1+
dak2+
gut2+
gpd1+
mRNA relative fold expression
WT
pka1Δ
pka1Δ rst2Δ
pka1Δ atf1Δ
E
7% Glu ⟶ 3% Gly
WT
pka1Δ
pka1Δ rst2Δ
pka1Δ atf1Δ
Time (h): 0 2 0 2 0 2 0 2
kDa
Gld1-HA
Cdc2
- 48
- 35
Relative Units
ns
7% Glu ⟶ 0.04% Glu + 3% Gly
WT
rst2Δ
atf1Δ
Time (h): 0 2 0 2 0 2
kDa
Gld1-HA
Cdc2
- 48
- 35
Relative Units
F
7% Glu ⟶ 0.04% Glu + 3% Gly
gld1+
dak1+
dak2+
gut2+
gpd1+
mRNA relative fold expression
0 2 0 2 0 2 (h)
WT
rst2Δ
atf1Δ
G
7% Glu ⟶ 0.04% Glu + 3% Gly
WT
gld1Δ
dak1Δ dak2Δ
Time (h): 0 5 7 0 5 7 0 5 7
kDa
CFP-Atg8
CFP
Cdc2
- 48
- 25
- 35
CFP-Atg8 proteolysis (%)
ns
H
7% Glu ⟶ 3% Gly
pka1Δ
pka1Δ gld1Δ
pka1Δ dak1,2Δ
Time (h): 0 5 7 0 5 7 0 5 7
kDa
CFP-Atg8
CFP
Cdc2
- 48
- 25
- 35
CFP-Atg8 proteolysis (%)

Figure 5

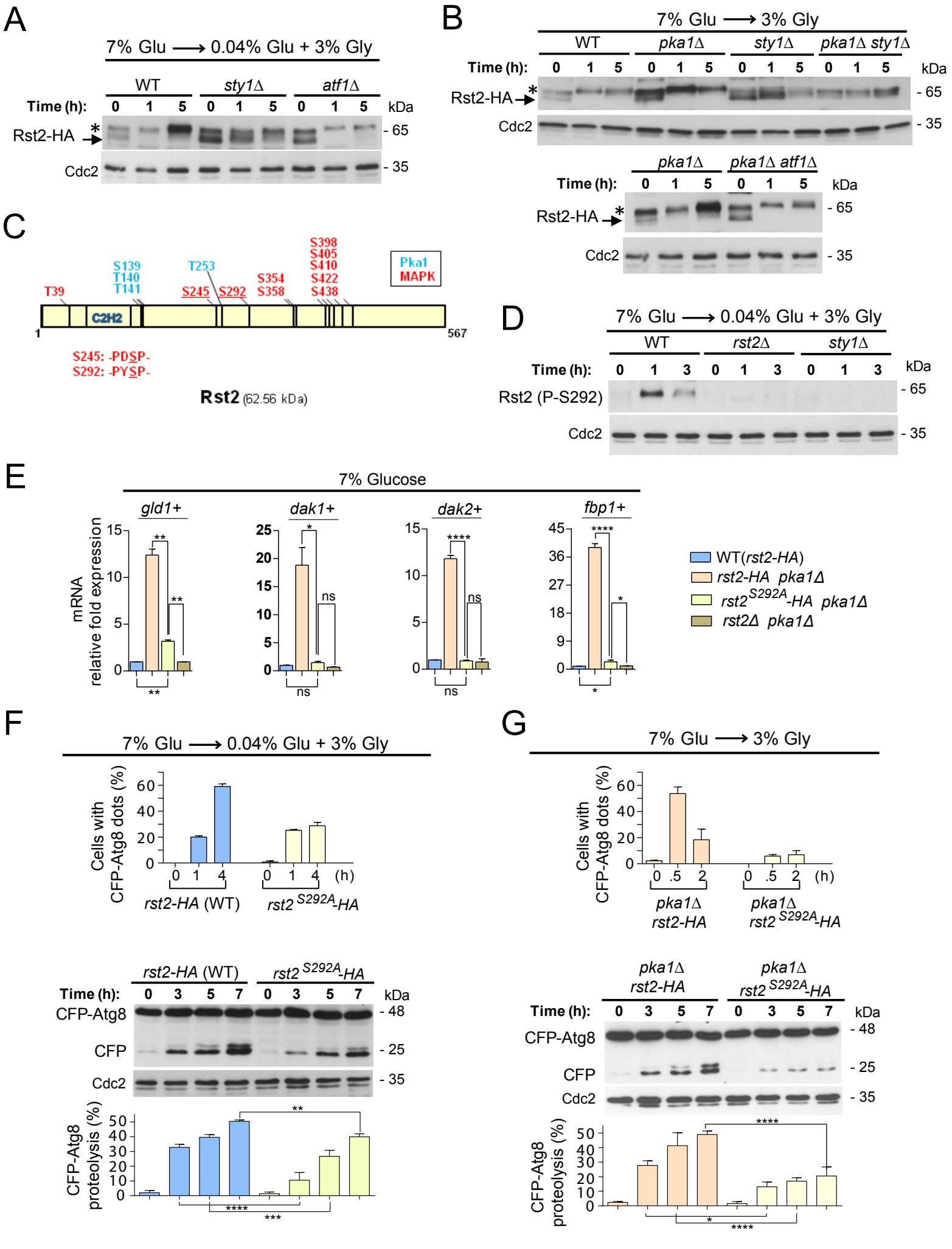
A
7% Glu ⟶ 0.04% Glu + 3% Gly
WT
sty1Δ
atf1Δ
Time (h):
0 1 5 0 1 5 0 1 5
kDa
Rst2-HA
- 65
Cdc2
- 35
B
7% Glu ⟶ 3% Gly
WT
pka1Δ
sty1Δ
pka1Δ sty1Δ
Time (h):
0 1 5 0 1 5 0 1 5 0 1 5
kDa
Rst2-HA
- 65
Cdc2
- 35
pka1Δ
pka1Δ atf1Δ
Time (h):
0 1 5 0 1 5
kDa
Rst2-HA
- 65
Cdc2
- 35
C
T39
S139
T140
T141
T253
S245
S292
S354
S358
S398
S405
S410
S422
S438
Pka1
MAPK
C2H2
1
567
S245: -PDSP-
S292: -PYSP-
Rst2 (62.56 kDa)
D
7% Glu ⟶ 0.04% Glu + 3% Gly
WT
rst2Δ
sty1Δ
Time (h):
0 1 3 0 1 3 0 1 3
kDa
Rst2 (P-S292)
- 65
Cdc2
- 35
E
7% Glucose
gld1+
dak1+
dak2+
fbp1+
mRNA relative fold expression
WT(rst2-HA)
rst2-HA pka1Δ
rst2S292A-HA pka1Δ
rst2Δ pka1Δ
F
7% Glu ⟶ 0.04% Glu + 3% Gly
Cells with CFP-Atg8 dots (%)
0 1 4 0 1 4 (h)
rst2-HA (WT)
rst2 S292A-HA
rst2-HA (WT)
rst2 S292A-HA
Time (h):
0 3 5 7 0 3 5 7
kDa
CFP-Atg8
- 48
CFP
- 25
Cdc2
- 35
CFP-Atg8 proteolysis (%)
G
7% Glu ⟶ 3% Gly
Cells with CFP-Atg8 dots (%)
0 .5 2 0 .5 2 (h)
pka1Δ rst2-HA
pka1Δ rst2 S292A-HA
pka1Δ rst2-HA
pka1Δ rst2 S292A-HA
Time (h):
0 3 5 7 0 3 5 7
kDa
CFP-Atg8
- 48
CFP
- 25
Cdc2
- 35
CFP-Atg8 proteolysis (%)

Figure 6

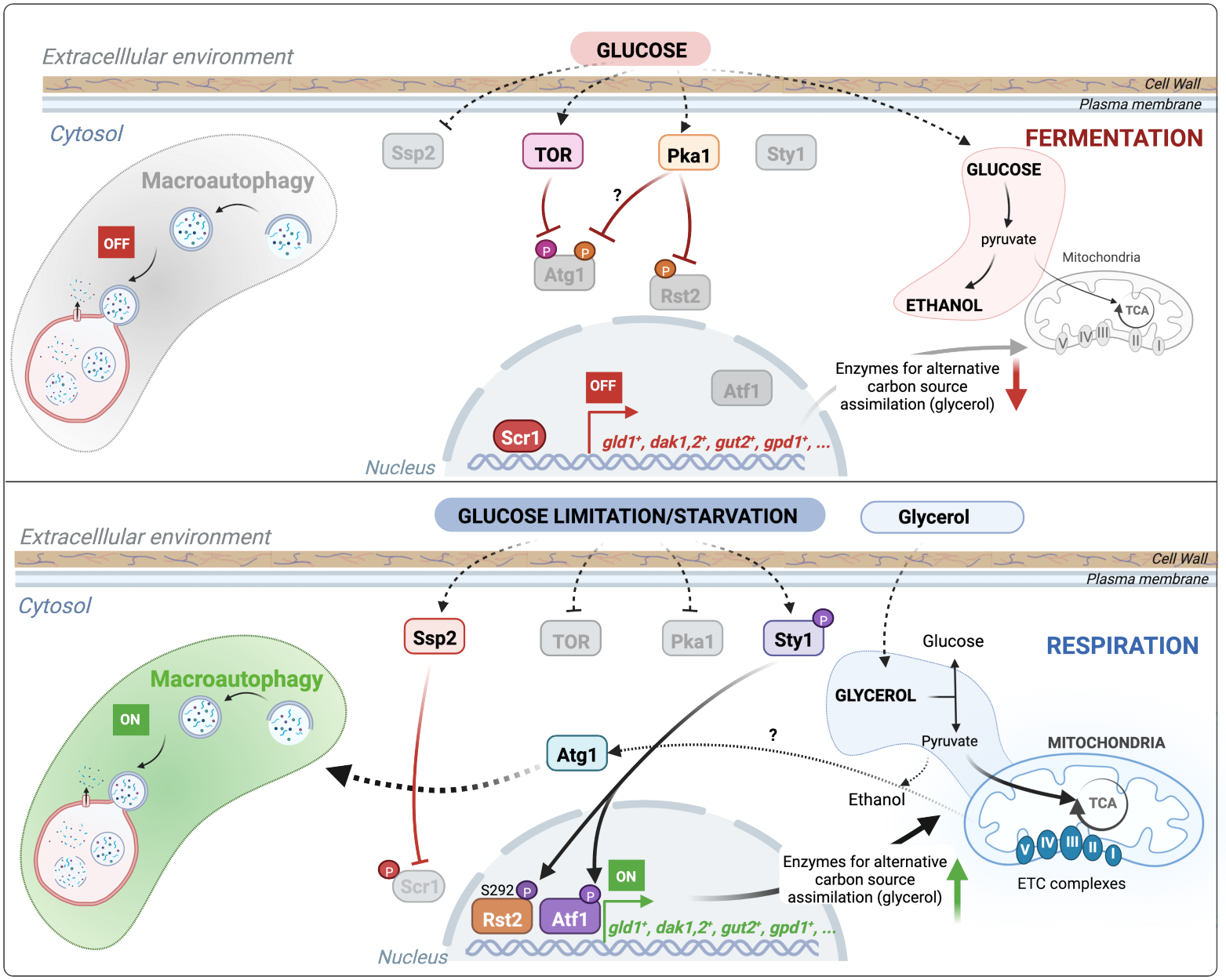
Extracelllular environment
GLUCOSE
Cell Wall
Plasma membrane
Cytosol
FERMENTATION
Ssp2
TOR
Pka1
Sty1
Macroautophagy
OFF
?
Atg1
Rst2
GLUCOSE
pyruvate
Mitochondria
ETHANOL
TCA
Enzymes for alternative carbon source assimilation (glycerol)
OFF
Atf1
Scr1
gld1+, dak1,2+, gut2+, gpd1+, ...
Nucleus
GLUCOSE LIMITATION/STARVATION
Glycerol
Extracelllular environment
Cell Wall
Plasma membrane
Cytosol
Ssp2
TOR
Pka1
Sty1
Glucose
RESPIRATION
Macroautophagy
ON
GLYCEROL
Pyruvate
MITOCHONDRIA
Atg1
?
Ethanol
TCA
Scr1
S292
ON
Rst2
Atf1
Enzymes for alternative carbon source assimilation (glycerol)
ETC complexes
gld1+, dak1,2+, gut2+, gpd1+, ...
Nucleus

Figure 7

Supplementary Information

cAMP-Protein Kinase A and Stress-Activated MAP Kinase signaling mediate transcriptional control of autophagy in fission yeast during glucose limitation or starvation

Armando Jesús Pérez-Díaz, Beatriz Vázquez-Marín, Jero Vicente-Soler, Francisco Prieto-Ruiz, Teresa Soto, Alejandro Franco, José Cansado* and Marisa Madrid*

TABLE OF CONTENTS

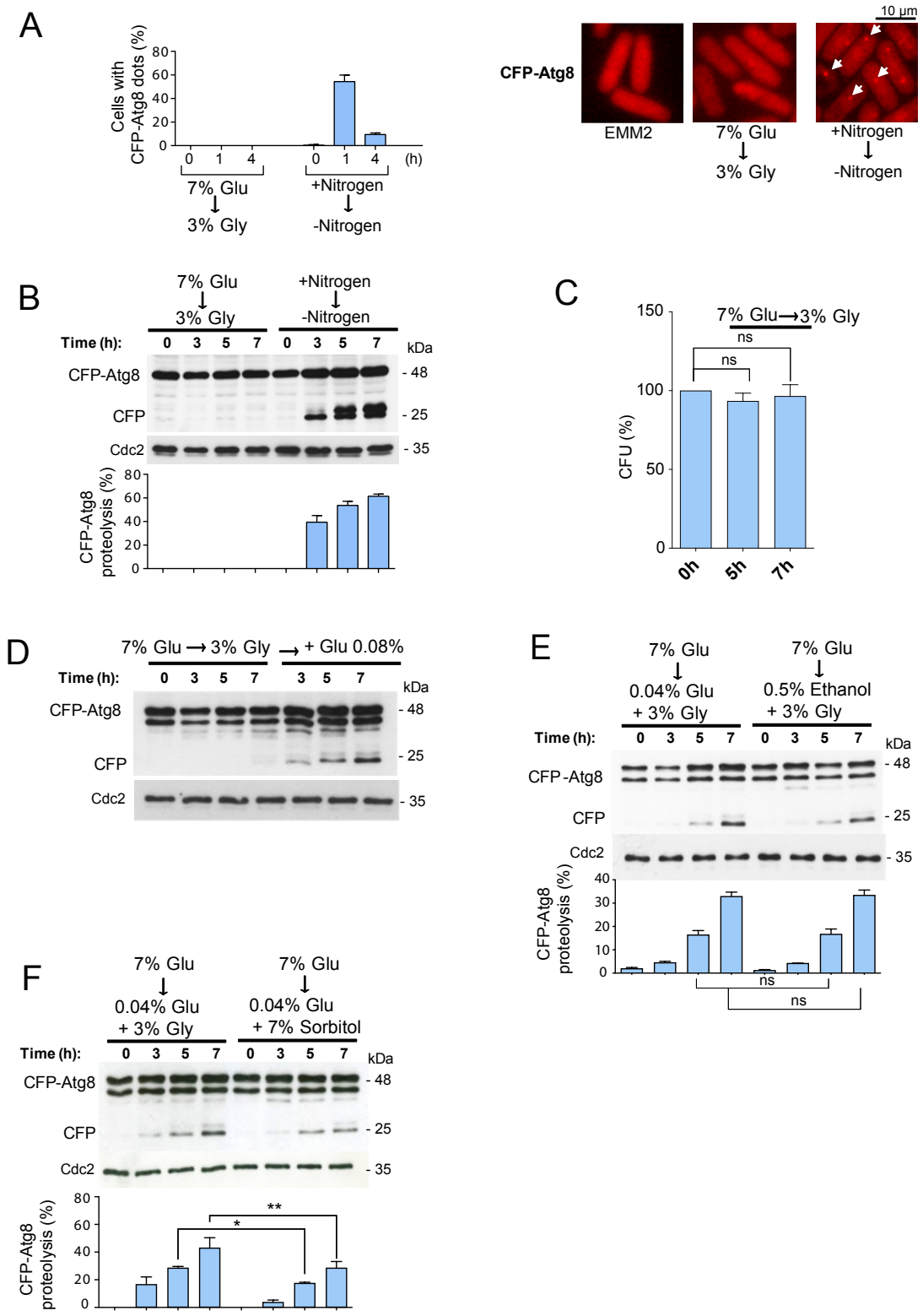

Figure S1. *S. pombe* cells do not undergo autophagy upon glucose starvation. (**A**) Right: Exponentially growing *S. pombe* wild-type cells expressing a CFP-Atg8 fusion were grown

in EMM2 with 7% glucose (Glu) and EMM2 plus nitrogen source, were recovered by filtration, and resuspended for the indicated times in the same medium in the presence of 3% glycerol (Gly) or lacking nitrogen source. The percentage of cells with visible CFP-Atg8 puncta was estimated at each time point by fluorescence microscopy (number of cells $\geq$300; three biological replicates) and is represented as mean $\pm$ SD. Left: Representative micrographs of cell samples after 3 h of incubation were observed by fluorescence microscopy. (**B**) Cell samples from the indicated time points were extracted with TCA, subjected to western blot analysis with anti-GFP antibody (CFP-Atg8 fusion and proteolysis), and normalized with anti-Cdc2 (internal loading control). CFP-Atg8 proteolysis was quantified by determining the signal ratio of the CFP-Atg8 band with respect to the free CFP band. Data are shown as mean $\pm$ SD, and correspond to biological triplicates. (**C**) Exponentially growing *S. pombe* wild-type cells expressing a CFP-Atg8 fusion were grown in EMM2 with 7% glucose, were recovered by filtration, and resuspended for the indicated times in the same medium in the presence of 3% glycerol. The relative percentage of colony formations by yeast cells was calculated as follows: CFU (%)=(CFU number of glycerol grown cells)/(CFU number of glucose grown cells)x100. All values are the average of three technical replicates. ns, not significant, as calculated by one-way ANOVA. (**D**) Exponentially growing *S. pombe* wild-type cells expressing CFP-Atg8 were grown in EMM2 with 7% glucose, were recovered by filtration, and resuspended for the indicated times in the same medium in the presence of 3% glycerol. After 7 h, glucose was added the medium at a final concentration of 0.08%. Results from representative experiments are shown. (**E**) Exponentially growing *S. pombe* wild-type cells expressing CFP-Atg8 were grown in EMM2 with 7% glucose, were recovered by filtration, and resuspended for the indicated times in the same medium in the presence of 0.04% Glu plus 3% Gly or 0.5% ethanol plus 3% Gly. Data for CFP-Atg8 proteolysis are shown as mean ± SD, and correspond to biological triplicates. ns, not significant, as calculated by one-way

ANOVA. (**F**) Exponentially growing *S. pombe* wild-type cells expressing CFP-Atg8 were grown in EMM2 with 7% glucose, were recovered by filtration, and resuspended for the indicated times in the same medium in the presence of 0.04% Glu plus 3% Gly or 0.04% Glu plus 7% Sorbitol. Data for CFP-Atg8 proteolysis are shown as mean ± SD, and correspond to biological triplicates. *, $p < 0.05$; **, $p < 0.01$, as calculated by one-way ANOVA.

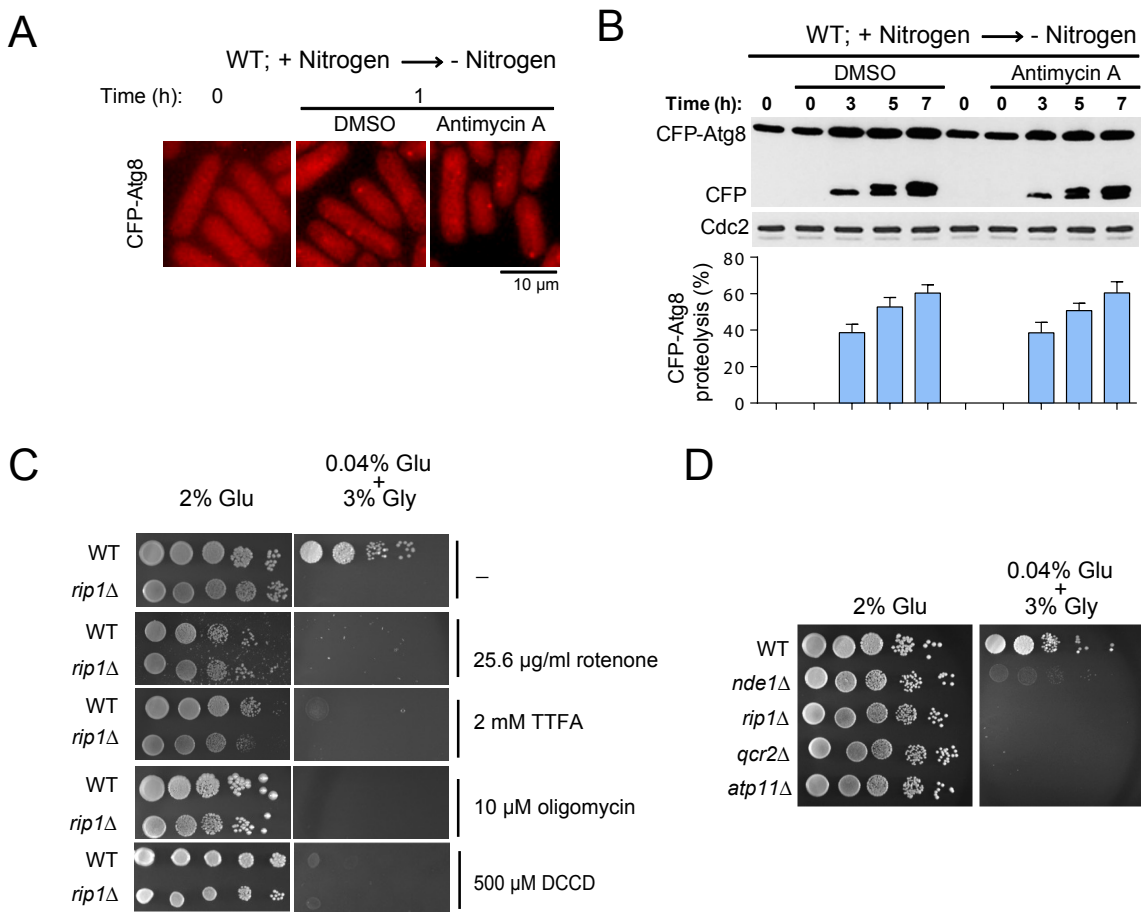

Figure S2. Autophagy is not inhibited by AA treatment when *S. pombe* is subjected to nitrogen starvation. (**A**) Exponentially growing *S. pombe* wild-type cells expressing a CFP-Atg8 fusion were incubated in the same medium lacking nitrogen source with or without 0.5 µM AA for 1 h and then observed through fluorescence microscopy. (**B**) Exponentially growing *S. pombe* wild-type cells expressing a CFP-Atg8 fusion were incubated in medium lacking nitrogen with or without 0.5 µM AA for the indicated times. Cell samples were extracted with TCA and subjected to western blot analysis with anti-GFP antibody (CFP-Atg8 fusion and proteolysis) and normalized with anti-Cdc2 (internal loading control). Data for CFP-Atg8 proteolysis are shown as mean ± SD and correspond to biological triplicates. (**C**) Decimal dilutions of strains of the indicated genotypes were spotted on YES solid plates with

2% Glu or 0.04% Glu plus 3% Gly with either 25.6 μg/ml rotenone, 2 mM TTFA, 10 μM oligomycin, or 500 μM DCCD. The plates were incubated at 30ºC for 3 days, and photographed. A representative experiment is shown. (**D**) Decimal dilutions of strains of the indicated genotypes were spotted on YES solid plates with 2% Glu or 0.04% Glu plus 3% Gly. The plates were incubated at 30ºC for 3 days, and photographed. A representative experiment is shown.

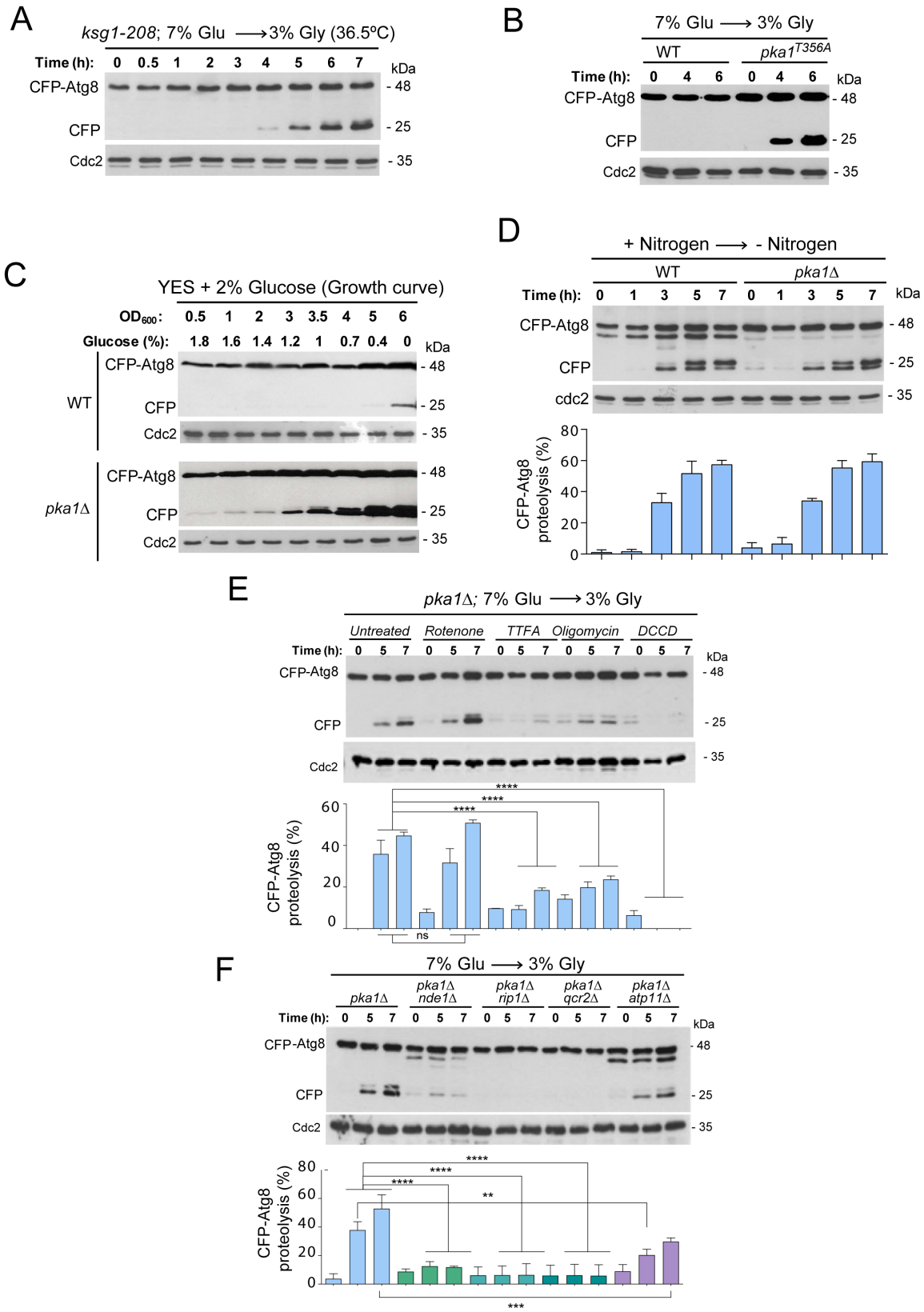

Figure S3. cAMP-PKA signaling represses *S. pombe* autophagy flux during the transition from fermentative to respiratory metabolism. (**A**) Exponentially growing *S. pombe ksg1-208*

cells expressing a CFP-Atg8 fusion were grown in EMM2 with 7% glucose (Glu), recovered by filtration, and resuspended at 36.5ºC for the indicated times in the same medium lacking glucose with 3% glycerol (Gly). Cell samples from the indicated time points were extracted with TCA, subjected to western blot analysis with anti-GFP antibody (CFP-Atg8 fusion and proteolysis), and normalized with anti-Cdc2 (internal loading control). Results from representative experiments are shown. (**B**) CFP-Atg8 fusion and proteolysis were followed in wild-type and Pka1-T356A cells incubated in EMM2 lacking Glu with 3% Gly for the indicated times. Results from representative experiments are shown. (**C**) CFP-Atg8 fusion and proteolysis were followed during the growth curve in wild-type and *pka1*Δ cells incubated in YES medium with 2% Glu. The OD_{600} and remaining glucose concentration in each sample are indicated. Results from representative experiments are shown. (**D**) CFP-Atg8 fusion and proteolysis were followed in wild-type and *pka1*Δ cells incubated in EMM2 lacking nitrogen for the indicated times. Data for CFP-Atg8 proteolysis are shown as mean ± SD, and correspond to biological triplicates. (**E**) CFP-Atg8 proteolysis of exponentially growing *S. pombe pka1*Δ cells expressing a CFP-Atg8 fusion incubated in medium with 3% Gly without further treatment (untreated), or treated with either 25.6 μg/ml rotenone, 2 mM TTFA, 10 μM oligomycin, or 500 μM DCCD. Data for CFP-Atg8 proteolysis are shown as mean ± SD, and correspond to biological triplicates. ns, not significant, ****, $p < 0.0001$, as calculated by one-way ANOVA. (**F**) CFP-Atg8 proteolysis of exponentially growing cells of the indicated mutants expressing a CFP-Atg8 fusion and incubated in medium with 3% Gly. Data for CFP-Atg8 proteolysis are shown as mean ± SD, and correspond to biological triplicates. ****, $p < 0.0001$, ***, $p < 0.001$, **, $p < 0.01$, as calculated by one-way ANOVA.

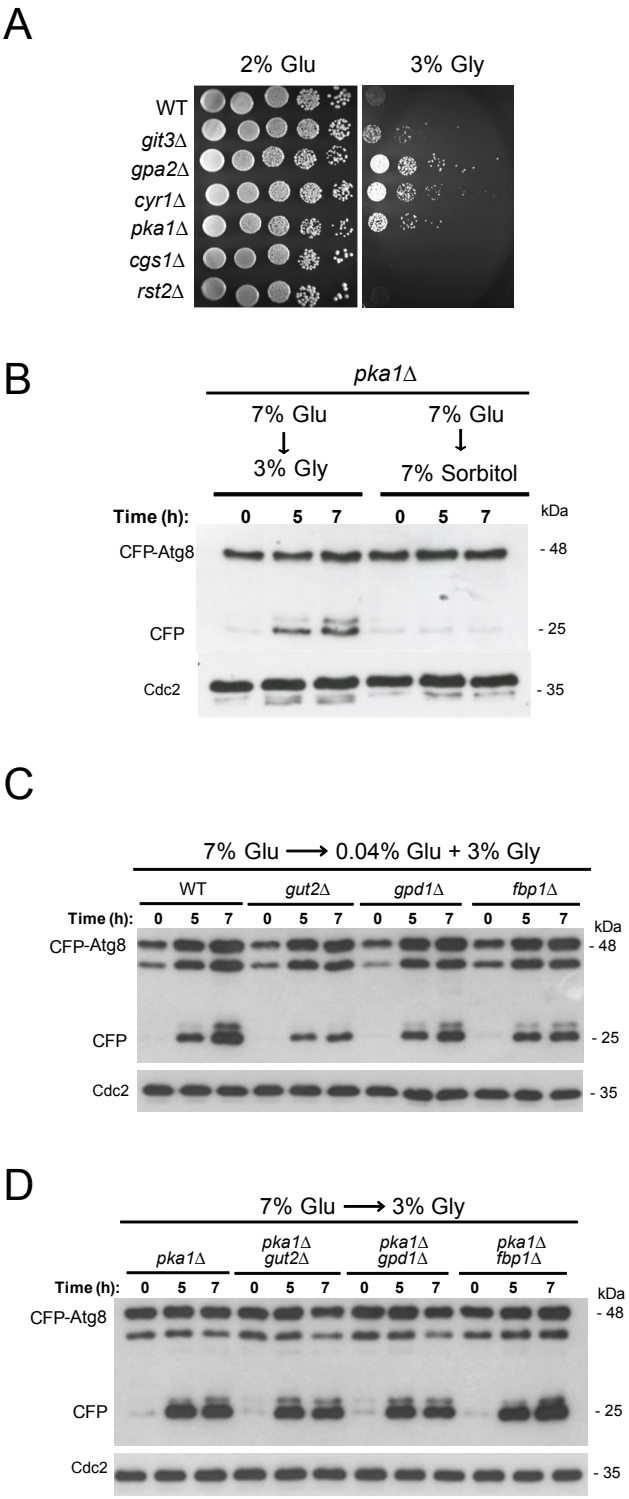

Figure S4. Deletion of *gut2*$^{+}$, *gpd1*$^{+}$, or *fbp1*$^{+}$ does not impair the autophagic flux of *S. pombe* cells upon glucose limitation or starvation. (**A**) Decimal dilutions of strains of the indicated genotypes were spotted on YES solid plates with 2% Glu or 3% Gly. The plates were

incubated at 30ºC for 3 days, and photographed. A representative experiment is shown. (**B**) Exponentially growing *S. pombe pka1*Δ cells expressing CFP-Atg8 were grown in EMM2 with 7% glucose, were recovered by filtration, and resuspended for the indicated times in the same medium in the presence of 3% Gly or 7% Sorbitol. Results from representative experiments are shown. (**C**) Exponentially growing *S. pombe* strains of the indicated genotypes expressing a CFP-Atg8 fusion were grown in EMM2 with 7% glucose (Glu) and resuspended in the same medium with 0.04% glucose plus 3% glycerol (Gly). CFP-Atg8 fusion and proteolysis were monitored at the indicated times by western blot analysis with anti-GFP antibody and normalized with anti-Cdc2 (internal loading control). Results from a representative experiment are shown. (**D**) CFP-Atg8 proteolysis of exponentially growing cells of the indicated mutants expressing a CFP-Atg8 fusion and incubated in medium with 3% Gly. Results from a representative experiment are shown.

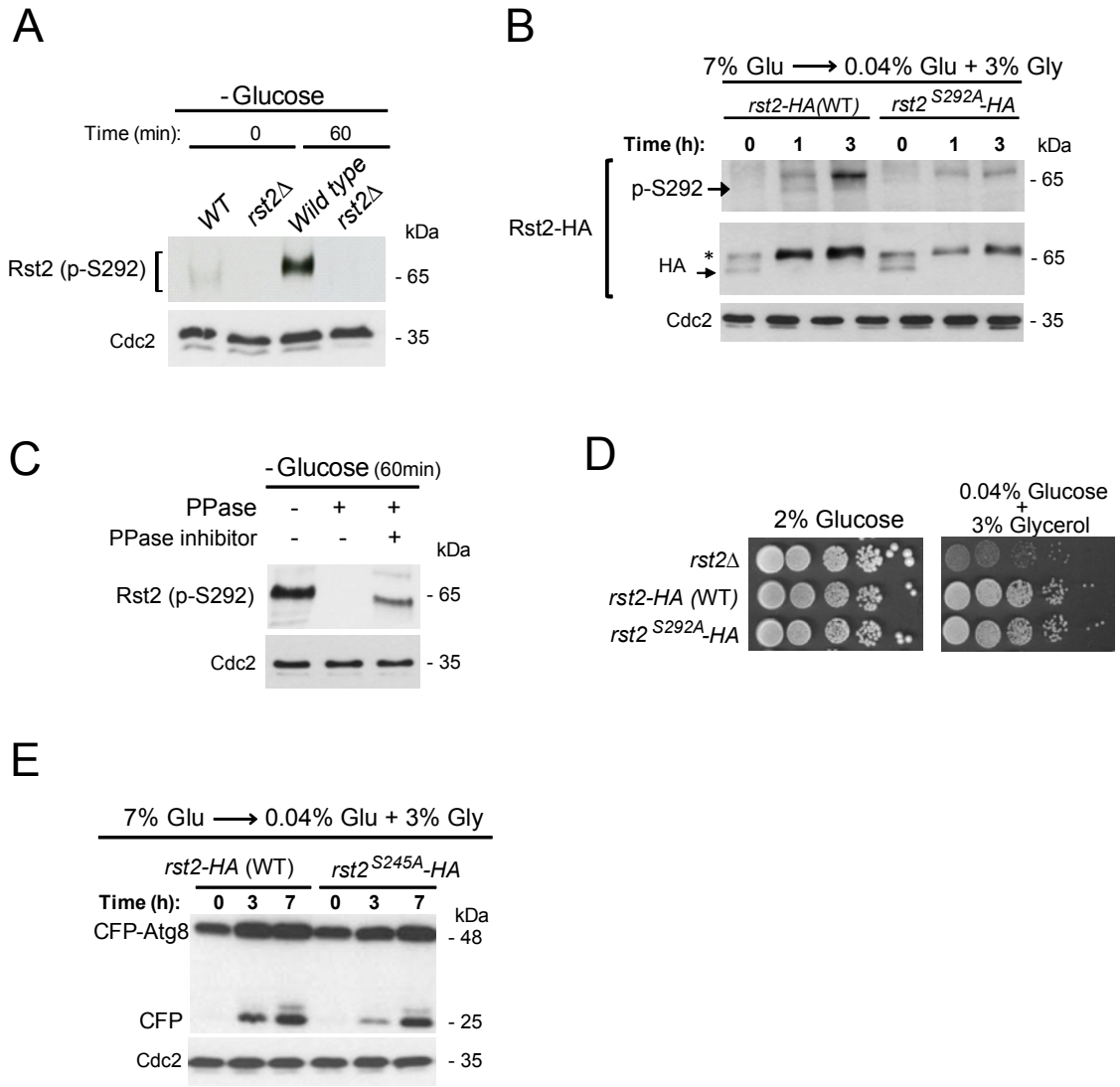

Figure S5. Functional characterization of *in vivo* Sty1-dependent phosphorylation of Rst2 at S292. (**A**) *In vivo* Rst2 phosphorylation at S292 was detected after immunoblotting with anti-phospho-S292 antibody of total native extracts of wild-type and *rst2Δ* cells growing exponentially in glucose-rich medium, and after glucose starvation for 60 min. Anti-Cdc2 was used as a loading control. Results from a representative experiment are shown. (**B**) Both total Rst2-HA levels and *in vivo* phosphorylation at S292 were detected in urea-denatured protein extracts from the indicated strains resuspended in EMM2 with 0.04% glucose (Glu) plus 3%

glycerol (Gly) for the indicated times after immunoblotting with anti-HA and anti-phospho-S292 antibodies, respectively. Anti-Cdc2 was used as a loading control. Results from a representative experiment are shown. "*" indicates the lower mobility and hyperphosphorylated protein band. (**C**) *In vivo* Rst2 phosphorylation at S292 was detected after immunoblotting with anti-phospho-S292 antibody of total native extracts of glucose-starved wild-type cells before and after treatment with lambda phosphatase in the presence or absence of a PPase-specific inhibitor. Anti-Cdc2 was used as a loading control. Results from a representative experiment are shown. (**D**) Decimal dilutions of strains of the indicated genotypes were spotted on YES solid plates with 2% Glu or 0.04 Glu plus 3% Gly. The plates were incubated at 30ºC for 3 days, and photographed. A representative experiment is shown. (**E**) Exponentially growing *S. pombe* Rst2-HA (WT) and Rst2-S245A-HA cells expressing a CFP-Atg8 fusion were grown in EMM2 with 7% Glu, and incubated in the same medium with 0.04% Glu plus 3% Gly for the indicated times. CFP-Atg8 fusion and proteolysis were monitored at the indicated times by western blot analysis with anti-GFP antibody and normalized with anti-Cdc2 (internal loading control). Results from a representative experiment are shown.

Table S1. *S. pombe* strains used in this work.

Strain	Genotype	Source
Figure 1		
AI030	*h- CFP-atg8:leu1*	Sun L-L, et al. (2013)
AJ311	*h- CFP-atg8:leu1 atg1::natMX6*	This work
AJ312	*h- CFP-atg8:leu1 atg11::kanMX6*	This work
AI035	*h? CFP-atg8:leu1 atg4::natMX6*	This work
AI036	*h? CFP-atg8:leu1 atg5::natMX6*	This work
AJ340	*h+ atg1-HA:kanMX6*	This work
Figure 2		
AJ163	*h? CFP-atg8:leu1 nde1::natMX6*	This work
AJ26	*h? CFP-atg8:leu1 rip1::natMX6*	This work
AJ27	*h? CFP-atg8:leu1 qcr2::natMX6*	This work
AJ166	*h? CFP-atg8:leu1 atp11::natMX6*	This work
BV1100	*h+ rad3::kanMX6*	Bioneer
AJ478	*h? CFP-atg8:leu1 rad3::kanMX6*	This work
AJ974	*h+ ssp2::ura4 (prototrofa)*	Sergio Moreno.
AJ1004	*h? CFP-atg8:leu1 ssp2::ura4*	This work
Figure 3		
AJ306	*h? CFP-atg8:leu1 git3::kanMX6*	This work
AJ361	*h? CFP-atg8:leu1 gpa2::kanMX6*	This work
AJ308	*h? CFP-atg8:leu1 cyr1::kanMX6*	This work
AJ332	*h? CFP-atg8:leu1 pka1::kanMX6*	This work
AJ956	*h? atg1-HA:KanMX6 pka1:: NatMX6*	This work
AI005	*h+CFP-atg8: leu1 cgs1:kanMX6*	This work
Figure 4		
AJ176	*h+ CFP-atg8:leu1 rst2:: natMX6*	This work
AJ335	*h+ CFP-atg8:leu1 pka1:: kanMX6 rst2::natMX6*	This work
BV1343	*h- rst2-3HA:NatMX6 (prototrofa)*	YGRC (FY32541)(JB729)
BV1344	*h- rst2.M3-3HA:NatMX6 (ura4+)*	YGRC (FY32542)(JB731)
AJ021	*h- CFP-atg8:leu1 rst2-3HA:natMX6*	This work
AJ023	*h? CFP-atg8:leu1 rst2-3HA:natMX6 pka1::kanMX6*	This work
AJ287	*h- CFP-atg8:leu1 rst2.M3-3HA:natMX6*	This work
AJ956	*h? CFP-atg8:leu1 rst2.M3-3HA:natMX6 cgs1:kanMX6*	This work
AJ084	*h+ CFP-atg8:leu1 sty1::natMX6*	This work
BV981	*h- CFP-atg8:leu1 sty1::natMX6 pka1::kanMX6*	This work
AJ168	*h- atf1::ura4*	YGRC (FY20910)(MY6940)
AJ194	*h? CFP-atg8:leu1 atf1::ura4*	This work
AJ208	*h? CFP-atg8:leu1 pka1::natMX6 atf1::ura4*	This work
Figure 5		
AJ910	*h- gld1-HA:hphMX6*	This work
AJ944	*h? gld1-HA:hphMX6 pka1::kanMX6*	This work
AJ941	*h? gld1-HA:hphMX6 atf1:ura4*	This work
AJ942	*h? gld1-HA:hphMX6 rst2:: NatMX6*	This work
AJ1012	*h? gld1-HA:hphMX6 atf1:ura4 pka1::kanMX6*	This work
AJ1017	*h? gld1-HA:hphMX6 rst2:: natMX6 pka1::KANMX6*	This work
AJ829	*h+ gld1::kanMX6*	Bioneer
AJ919	*h+ dak1:.kanMX6*	Bioneer
AJ920	*h+ dak2::kanMX6*	Bioneer
AJ879	*h? CFP-atg8:leu gld1::kanMX6*	This work
AJ882	*h? CFP-atg8:leu gld1::kanMX6 pka1::natMX6*	This work
AJ959	*h? CFP-atg8:leu1 dak1::kanMX6 dak2::hphMX6*	This work
AJ965	*h? CFP-atg8:leu1 dak1::kanMX6 dak2::hphMX6 pka1::natMX6*	This work
Figure 6		
AJ488	*h+ isp6::kanMX6*	Bioneer
AJ734	*h? CFP-atg8:leu1 rst2-3HA:kanMX6 Isp6::hphMX6*	This work

AJ751	*h? CFP-atg8:leu1 rst2-3HA: kanMX6 Isp6:: hphMX6 sty1::kanMX6*	This work
AJ767	*h? CFP-atg8:leu1 rst2-3HA: kanMX6 Isp6::hphMX6 atf1::ura4*	This work
AJ737	*h? CFP-atg8:leu1 rst2-3HA:kanMX6 Isp6::hphMX6 pka1::natMX6*	This work
AJ755	*h? CFP-atg8:leu1 rst2-3HA:kanMX6 Isp6:: hphMX6 sty1::kanMX6 pka1::natMX6*	This work
MM1	*h+*	Lab stock
AJ118	*h+ Rst2:: natMX6*	This work
AJ216	*h+ sty1:: kanMX6*	Lab Stock
AJ31	*h- CFP-atg8:leu1 rst2-3HA:kanMX6*	This work
AJ43	*h- CFP-atg8:leu1 rst2-3HA:kanMX6 pka1::natMX6*	This work
AJ34	*h- CFP-atg8:leu1 rst2(S292A)-3HA:kanMX6*	This work
AJ717	*h? CFP-atg8:leu1 rst2(S292A)-3HA:kanMX6 pka1::natMX6*	This work
Supplementary figures		
BV050	*h? ksg1-208*	Lab stock
BV973	*h? CFP-atg8:leu1 ksg1-208*	This work
BV945	*h- pka1 -13myc:KanMX6*	Lab stock
BV1026	*h? CFP-atg8:leu1 Pka1-13myc:KanMX6*	This work
BV925	*h90 pka1(T356A)-13myc:KanMX6*	Lab stock
BV1032	*h? CFP-atg8:leu1 pka1(T356A)-13myc:KanMX6*	This work
AJ164	*h? CFP-atg8:leu1 nde1::natMX6 pka1::kanMX6*	This work
AJ709	*h? CFP-atg8:leu1 rip1::natMX6 pka1::kanMX6*	This work
AJ713	*h? CFP-atg8:leu1 qcr2::natMX6 pka1::kanMX6*	This work
AJ167	*h? CFP-atg8:leu1 atp11::natMX6 pka1::kanMX6*	This work
AJ861	*h+ gut2::kanMX6*	Bioneer
AJ834	*h+ gpd1::kanMX6*	Bioneer
BV1087	*h+ fbp1::kanMX6*	Bioneer
AJ864	*h? CFP-atg8:leu1 gut2::kanMX6*	This work
AJ865	*h? CFP-atg8:leu1 gut2::kanMX6 pka1::natMX6*	This work
AJ869	*h? CFP-atg8:leu1 gpd1::kanMX6*	This work
AJ870	*h? CFP-atg8:leu1 gpd1::kanMX6 pka1::natMX6*	This work
AJ827	*h? CFP-atg8:leu1 fbp1::kanMX6*	This work
AJ828	*h? CFP-atg8:leu1 fbp1::kanMX6 pka1::natMX6*	This work
AJ32	*h? CFP-atg8:leu1 rst2(S245A)-3HA:kanMX6*	This work

*All strains are *ade- leu1-32 ura4-D18*

Table S2. Oligonucleotides used in this work.

NAME	Sequence
Atg1-del-R	ATTCATAACAAAATTTAGACTCAGAGCTCAGCTCATACAATATGCGAATTTGTTCAATAAAAGGGC GAAATCGTCGGTGTGAATTCGAGCTCGTTTAAAC
Atg1-del-F	TTGCCAACTCCCATGCTATCAAAGTGAGTATAAAGGCAGCTAAAACCCTTACACCTGTCTTATCGT GAACCAGAAGCTGTCGGATCCCCGGGTTAATTAA
Atg1-C-tag-R	ATTCATAACAAAATTTAGACTCAGAGCTCAGCTCATACAATATGCGAATTTGTTCAATAAAAGGGC GAAATCGTCGGTGTGAATTCGAGCTCGTTTAAAC
Atg1-C-tag-F	AATCGAAACAAATCCAGGCTAATGTAGCCAACAAAGTAACAGAAAGTGTTGCGAAAATAACACTTG CCCCCAATCTTGCTCGGATCCCCGGGTTAATTAA
Pka1-Del-5’	GGGTACTTTATAAGTTTGACGAACGATTAGTGAATTTTAATTATCTTTTCGTGTATAAACGCTATT TCACATTTGTACTCCGGATCCCCGGGTTAATTAA
Pka1-Del-3’	AACGTCACTTGCATTGCACTAAATCAAATAGGCATTCGTTGCTCAACGCTTTAAGGCAATAGTACA ATGAATCAATAAGCGAATTCGAGCTCGTTTAAAC
Rst2-Del-F	TTTGAATCCTGATTGCAATCACTTTCAAGCTTTATTTCCCTTCATATCTTTTATTTTAACAACATA TTCTTCTTTTGAAACGGATCCCCGGGTTAATTAA
Rst2-Del-R	CAGATCAATCCTTAAATTAATTAAAAACCGAATCAAAGCTAGTTGATTTTTGTTTAAAAAAACTAA AAGATGCATTTCATGAATTCGAGCTCGTTTAAAC
Rad3del-F	TAATTCTATTGAGATATTTTATTACTTACAATCGTCTTTTATAAATGCTCAAGACTTTGAACGCGC GTGTTGCGTTTTAACGGATCCCCGGGTTAATTAA
Rad3del-R	ACAAGAAATTGAACAACTCAGCGAGAATTCTTCATCGGATTAATAAATAAAATATCTTCGATTCAA ATCATAAGTTTAATGAATTCGAGCTCGTTTAAAC
Rst2-tag-F	GGTCTTCAGACTTTAATTATCCTGTATCCGAAACTTCCGGTTTGCTTACAGATAATAATCGGAATC AACCGCCCTCATTTCGGATCCCCGGGTTAATTAA
Rst2-tag-R	AGTTGATTTTTGTTTAAAAAAACTAAAAGATGCATTTCATTAAGAAACAAATAGTATAAAATATAA AGATATGAAAAAAAGAATTCGAGCTCGTTTAAAC
Qcr2(CIII)-DEL-F	CAACTCCCACCTCTGTTGCAAGCAGCGTAATTTAGTAAACACCGATTAAAAACTTTTTCGAAAAGT CCTAAATAGGTAATCGGATCCCCGGGTTAATTAA
Qcr2(CIII)-DEL-R	ACATCATCCTAAGCTTATGGTGTATAAAAAGTTTTCAAAGAAAGATTTTCGATAAAAAAAAAGATT TGTAGAGAAGTATCGAATTCGAGCTCGTTTAAAC
Rip1(CII)-DEL-R	GCTAAAGAAGAAGTAAAAGAGAGGGGAGAAAAAGGAGGGAGGAAATCAGCTAGGACAAAAGTTTTT GAGCGAAATAAATTGAATTCGAGCTCGTTTAAAC
Rip1(CII)-DEL-R	AGAGGCAGCTTGACGTTTCTTCCCCAACCGCTACCCACCGAATATTTCAACAACCTGTTTCTCTTT AAAACGTTGTAAAACGGATCCCCGGGTTAATTAA
Gld1-C-TAG-F	TCACAAAAATGGCAAGAACAAACTGGGATGGACCGAGCGTTTTAGATTACCCCCTTCTCGTCATAG TCCTCAGTTGACCGACATTCATCCACGGATCCCCGGGTTAATTAA
Gld1-C-TAG-R	TTAATGATCAATGAAGAAAACCCGCTTAAAAATTTCTTTTCTTCTTTTGGATTTACTAGGGAAAAT TGAAGCTGGGGATAAAAATAATGCGAATTCGAGCTCGTTTAAAC
Rst2-HA-Amplicon-F	CAGATCATTGAAGATTATTGCACTA
Rst2-HA-Amplicon-R	TTTCGCTAATAACTCCTTATTTGAC
Rst2-S245A-R	CGATAGTACAAAGGAGCGTCGGGTCCATAAGGC
Rst2-S245A-F	GCCTTATGGACCCGACGCTCCTTTGTACTATCG
Rst2-S292A-R	TGAAACGGCGTTAGGTGCATACGGCATTCTAGC
Rst2-S292A-F	GCTAGAATGCCGTATGCACCTAACGCCGTTTCA

Table S3. Microarray data and GO enrichments.

Data are available as a Figshare dataset (doi: 10.6084/m9.figshare.20732248).